THE ASTROPHYSICAL JOURNAL, 315:349–370, 1987 April 1

A COMPUTATIONAL CODE FOR TWO-DIMENSIONAL UNSTEADY MAGNETOHYDRODYNAMICS BY THE METHOD OF CHARACTERISTICS

Y. Q. LOU
Physics Department, Harvard University
R. ROSNER
Department of Astronomy, Harvard University
AND
P. ULMSCHNEIDER
Institut für Theoretische Astrophysik der Universität Heidelberg
Received 1986 January 24; accepted 1986 September 15

ABSTRACT

We present a computational code for solving two-dimensional, time-dependent magnetohydrodynamic (MHD) equations by the method of characteristics. Earlier computational work on two-dimensional hydrodynamic equations by the method of characteristics is generalized to include the presence of magnetic fields. The physical system under consideration is axisymmetric, with $v_\phi = 0$ and $B_\phi = 0$. The numerical scheme is described in detail, and the results of calculations are compared with two analytic solutions of the MHD equations: (*a*) linearized, standing MHD wave motions in a magnetized cylindrical plasma; (*b*) nonlinear self-similar expansion of a magnetized plasma ball. In addition, we have studied the nonlinear development of standing MHD wave solutions in a cylindrical plasma. Our results show that the method of characteristics, although complex to implement, can be successfully applied to solve the MHD equations, and that highly accurate, stable results can be obtained. These properties take on especial importance in light of the fact that the method developed here can be naturally embedded in the computational architecture of massively parallel processors.

Subject headings: hydromagnetics — plasmas

I. INTRODUCTION

Because of advances in computational power, and ready access to such power, it is now feasible to carry out direct numerical simulations of astrophysical magnetohydrodynamic (MHD) problems which have received only analytic treatment to date. One such problem deals with the nonlinear evolution of propagating and standing waves in an inhomogeneous gravitationally stratified conducting fluid. In particular, our interest centers on the generation and possible propagation of such waves in the presence of the intense magnetic flux tubes observed to be embedded in the solar atmosphere, a problem which has received much recent attention (see Spruit 1981; Spruit and Roberts 1983; Herbold *et al.* 1985). The purpose of this paper is to present the initial results of a new numerical code for solving such problems, namely one based on the method of characteristics implemented for a two-dimensional magnetofluid.

There are four basically different methods of numerical integration for hyperbolic partial differential equations developed to date: (i) the direct finite-difference method (Roache 1976), (ii) the finite-element method (Mitchell 1972; Deinzer *et al.* 1984), (iii) the pseudo-spectral method (Gottlieb and Orszag 1977; Fletcher 1984), and (iv) the method of characteristics (Richardson 1964). The method of characteristics has particular appeal for numerical integration of equations describing physical phenomena because it relates to conditions on loci of points along which physical disturbances travel. However, the programming logic is generally quite complex and hence involves an extensive programming effort. This complexity, however, is potentially offset by the fact that, whereas the method of characteristics can be embedded only awkwardly on a serial processor, it embeds naturally on a parallel processor because the iterations for physical variables at each grid point along the associated characteristic cone proceed independently.

Our strategy is as follows: in the present paper, we discuss the basic algorithm and demonstrate explicitly that an accurate numerical code can be implemented. In order to test our code, we have compared the results of our code with analytic solutions to the MHD equations for two distinct problems. The first is for linearized, standing MHD wave motions in a magnetized cylindrical plasma with prescribed boundary conditions on top, bottom, and wall of the cylinder. The second is for nonlinear, self-similar expansion of a magnetized plasma ball (Low 1982). In addition, we study the nonlinear development of large-amplitude standing MHD wave solutions; this study includes tests of the conservation laws of energy, mass, and magnetic flux. At the present stage of development of the code, the treatment of shocks is incomplete, and the implementation of shock finding and following is the task of ongoing development.

The outline of the paper is as follows. In § II, the basic MHD equations are given, while the theory of characteristics in two-dimensional MHD is briefly discussed in § III. In § IV, the MHD equations are cast into characteristic form on the fast cone and along the fluid line; the numerical procedure is described in detail in the following section. The treatment of the boundary conditions is an important subject in its own right, and § VI is devoted to this problem. The tests of our code are carried out in § VII. Our discussions and conclusions are given in § VIII.

II. BASIC MAGNETOHYDRODYNAMIC EQUATIONS

We generalize the previous computational work on two-dimensional hydrodynamic equations by the method of characteristics (Richardson 1964; Stefanik *et al.* 1984) to include the effects of magnetic fields. In the one-dimensional case, the partial differential equations can be reduced to ordinary differential equations along the characteristics, where the derivatives normal to the characteristics disappear. For nonlinear equations, the characteristic lines are functions of the solution to be obtained and cannot be determined *a priori*. For the two-dimensional case, further complications arise. In general, by appropriate cordinate transformation, the original differential equations can be reduced to partial differential equations with one independent variable less on the characteristic surfaces where the derivatives normal to the characteristic surfaces disappear. However, it is usually difficult to express explicitly the partial differential equations thus obtained in terms of the independent coordinate variables on the characteristic surface. As in the one-dimensional case for nonlinear equations, the determination of the characteristic cone (Fig. 1), which is the envelope of the characteristic surfaces, depends on the solution of the equations to be obtained.

For a given spatial grid, the time step for integration is chosen with the following concerns in mind: (i) the local characteristic cone must be accurately constructed from the information at the previous time step, and the MHD equations must be expressed on this cone (this is essentially the Courant condition); (ii) for convergence and stability of a specific numerical scheme, experience and theoretical analysis using the Von Neumann condition in the linear regime of the equations (Richtmyer 1957; Shin and Kot 1978) show that the time step must be less than the Courant time step (the precise definition of the Courant time step in the MHD case will be given later). A further constraint on the size of the time step follows from the fact that the set of MHD equations dealt with here can be expanded in a power series in time when the initial spatial dependence of a wave perturbation is given. From the Cauchy–Kowalewski theorem (Garabedian 1964), this expansion must converge to a unique solution in some neighborhood of the initial time; that is, we do not expect that the convergence domain of the expansion is infinite, so that depending on the parameter regime, a finite convergence domain can be found in principle. Since any numerical scheme for the MHD equations is in essence a kind of expansion in time, the finite convergence domain in time sets up another intrinsic upper bound for the time step in the numerical integration.

In general, we cast the MHD equations into characteristic form on the characteristic cones and along the fluid line, and then write down their corresponding finite difference forms. In the present scheme, the physical variables are advanced in time, and the coefficients of the time derivatives of the physical variables and the "source terms" involving the spatial derivatives in the equations are approximated by the arithmetic means of their values at the new and the old time steps. This is an implicit scheme, through which the values of the physical variables at the new time step are obtained by numerical iteration. With the numerical scheme described above, the derivatives of the unknown variables at the new time step are introduced, and different directions along the characteristic cones are chosen to obtain enough equations to solve for these unknowns. We have used the fast cone and the fluid line to express all of these equations.

The reason for using the fast cone alone, but not the slow

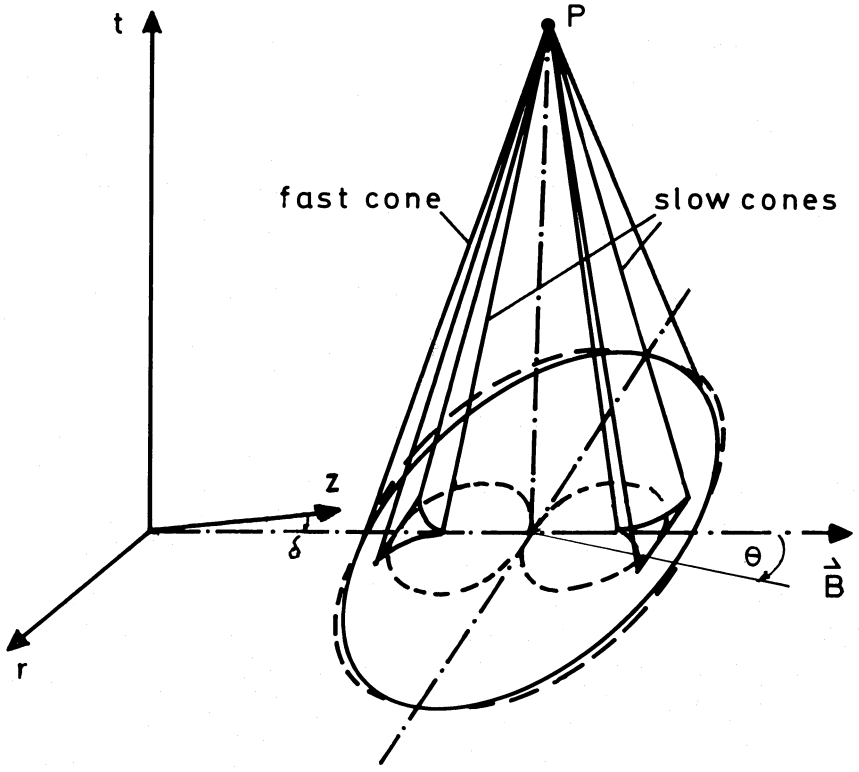

FIG. 1.—Basic geometric structures of the MHD fast and slow wave cones for a uniform and homogeneous background magnetic field; dashed line represents the cones for the fast and slow phase velocities, and solid line represents the cones for the fast and the group velocities.

cone (see Fig. 1), is the following. Although it is common to think of the fast and slow cones as separate entities, the fact is that they are uniquely related; i.e., for a locally homogeneous background, the shape of the slow cone is entirely determined by the shape of the fast cone, and vice versa. The crucial point here is that the fast cone contains as much background information as the slow cone does. Thus, choosing the bicharacteristics along the fast cone is not essentially different from choosing those along the slow cones. However, several benefits accrue by using the fast cone. First, the fast cone resembles the Mach cone in the hydrodynamic case, and the MHD treatment of the finite difference equations is similar to that for the hydrodynamic case. Second, the fast cone covers a larger area than the slow cone does, so that the numerical error introduced by subtraction of values at different points on the fast cone is less than that on the slow cone. Third, when the magnetic field is reduced to zero, the fast cone reduces to the Mach cone and the slow cone vanishes. If some of the finite difference equations were expressed along the slow cone, it would be difficult to handle situations where the magnetic field is small or zero. In other words, to express the finite difference equations along the fast cone is more general.

We use the ideal MHD equations to describe the adiabatic motions of a nonviscous, infinitely conducting, magnetized fluid. The basic equations are the following:

1. The momentum equation:

$$\rho\left[\frac{\partial \boldsymbol{v}}{\partial t} + (\boldsymbol{v}\cdot\nabla)\boldsymbol{v}\right] = -\nabla p + \frac{1}{4\pi}(\nabla\times\boldsymbol{B})\times\boldsymbol{B}\,. \tag{2.1}$$

2. The equation of continuity:

$$\frac{\partial \rho}{\partial t} + \nabla\cdot(\rho\boldsymbol{v}) = 0\,. \tag{2.2}$$

3. The induction equation:

$$\frac{\partial \boldsymbol{B}}{\partial t} = \nabla\times(\boldsymbol{v}\times\boldsymbol{B})\,. \tag{2.3}$$

4. The condition for adiabatic flow:

$$\frac{\partial}{\partial t}(p\rho^{-\gamma}) + (\boldsymbol{v}\cdot\nabla)(p\rho^{-\gamma}) = 0\,. \tag{2.4}$$

5. The divergence-free condition for the magnetic field:

$$\nabla\cdot\boldsymbol{B} = 0\,. \tag{2.5}$$

The quantities p, ρ, $\boldsymbol{v}$, and $\boldsymbol{B}$ are the gas pressure, density, velocity, and magnetic field, respectively. The constant γ is the ratio of the specific heats.

In cylindrical coordinates (r, ϕ, z) for an axisymmetric physical system, with $v_\phi = 0$ and $B_\phi = 0$ (see below), equations (2.1)–(2.4) can be written explicitly as follows:

$$\frac{\partial u}{\partial t} + u\frac{\partial u}{\partial r} + v\frac{\partial u}{\partial z} + \frac{1}{\rho}\frac{\partial p}{\partial r} - \frac{B_z}{4\pi\rho}\frac{\partial B_r}{\partial z} + \frac{B_z}{4\pi\rho}\frac{\partial B_z}{\partial r} = 0\,, \tag{2.6}$$

$$\frac{\partial v}{\partial t} + u\frac{\partial v}{\partial r} + v\frac{\partial v}{\partial z} + \frac{1}{\rho}\frac{\partial p}{\partial z} + \frac{B_r}{4\pi\rho}\frac{\partial B_r}{\partial z} - \frac{B_r}{4\pi\rho}\frac{\partial B_z}{\partial r} = 0\,, \tag{2.7}$$

$$\frac{\partial \rho}{\partial t} + \frac{1}{r}\frac{\partial}{\partial r}(r\rho u) + \frac{\partial}{\partial z}(\rho v) = 0\,, \tag{2.8}$$

$$\frac{\partial (p\rho^{-\gamma})}{\partial t} + u\frac{\partial}{\partial r}(p\rho^{-\gamma}) + v\frac{\partial}{\partial z}(p\rho^{-\gamma}) = 0\,, \tag{2.9}$$

$$\frac{\partial B_r}{\partial t} + u\frac{\partial B_r}{\partial r} + v\frac{\partial B_r}{\partial z} + B_r\frac{\partial v}{\partial z} - B_z\frac{\partial u}{\partial z} + \frac{uB_r}{r} = 0\,, \tag{2.10}$$

$$\frac{\partial B_z}{\partial t} + u\frac{\partial B_z}{\partial r} + v\frac{\partial B_z}{\partial z} - B_r\frac{\partial v}{\partial r} + B_z\frac{\partial u}{\partial r} + \frac{uB_z}{r} = 0\,, \tag{2.11}$$

$$\frac{1}{r}\frac{\partial}{\partial r}(rB_r) + \frac{\partial B_z}{\partial z} = 0\,, \tag{2.12}$$

where equation (2.12) has been used in equations (2.10) and (2.11). Combining equations (2.8) and (2.9), we have

$$\frac{\partial p}{\partial t} + u\frac{\partial p}{\partial r} + v\frac{\partial p}{\partial z} + \rho a^2\left(\frac{\partial u}{\partial r} + \frac{\partial v}{\partial z} + \frac{u}{r}\right) = 0\,, \tag{2.13}$$

where $a^2 \equiv \gamma p/\rho$, u is the r-component velocity, and v is the z-component velocity.

The main reason for setting both v_ϕ and B_ϕ to zero is simplicity. One obvious consequence of this assumption for an axisymmetric system is the exclusion of the transverse (Alfvén) mode. In principle, v_ϕ and B_ϕ can be included for axisymmetric systems by adding two more equations for the time evolution of v_ϕ and B_ϕ, and there do exist corresponding linear analytical solutions which can be used for testing. This complication will be considered in a separate publication.

The set of equations (2.1)–(2.5) is of hyperbolic nature and can be cast into characteristic form on the fast cone. The same is true for the set of equations (2.6)–(2.13). We shall describe the theory of characteristics in the next section.

III. THE THEORY OF CHARACTERISTICS IN TWO-DIMENSIONAL MHD

In this section, the theory of characteristics in its basic form is illustrated by the propagation of linearized MHD wave motions in a homogeneous medium, and its application to the numerical procedure for general nonlinear MHD motions in an inhomogeneous medium is outlined. To clarify matters, we first consider a uniform, stationary background, i.e., in the absence of background flow, the background gas pressure p_0, density ρ_0, and magnetic field $\boldsymbol{B}_0$ are constants independent of time and space. The equations of motion given by equations (2.1)–(2.5) are of hyperbolic nature. When the physical system is perturbed at a point, the linearized version of equations (2.1)–(2.5) shows that three distinct wave modes are excited, whose characteristic phase velocities are

$$C_f = \{\tfrac{1}{2}[a^2 + b^2 + \sqrt{(a^2+b^2)^2 - 4a^2b^2\cos^2\theta}]\}^{1/2}\,, \tag{3.1}$$

$$C_s = \{\tfrac{1}{2}[a^2 + b^2 - \sqrt{(a^2+b^2)^2 - 4a^2b^2\cos^2\theta}]\}^{1/2}\,, \tag{3.2}$$

$$C_t = b|\cos\theta|\,, \tag{3.3}$$

where $a^2 \equiv \gamma p_0/\rho_0$ is the square of the sound speed, $b^2 \equiv |\boldsymbol{B}_0|^2/4\pi\rho_0$ is the square of the Alfvén speed, and θ is the angle between the wave vector and the magnetic field. The phase velocities C_f, C_s, and C_t are those of fast, slow, and transverse modes, respectively. Since the physical system is axisymmetric about the direction of the background magnetic field $\boldsymbol{B}_0$, the expressions (3.1)–(3.3) for C_f, C_s, and C_t are valid for any plane containing the magnetic field $\boldsymbol{B}_0$. The propagation behavior of the modes is usually displayed by means of polar diagrams (Friedrichs diagrams; see Jeffrey and Taniuti 1964), in which the radial distance represents the magnitude of the phase velocity and the direction of the radial vector is that of the wave vector.

Expressions (3.1)–(3.3) describe anisotropic phase propagation of MHD waves. Physically, the more pertinent representation of these waves in an anisotropic medium are the corresponding group velocities with which disturbance patterns propagate (see Fig. 1). The physical interpretation, the geometrical construction, and the mathematical formulae of the MHD group velocities are discussed by Courant and Hilbert (1962, p. 551), Jeffrey and Taniuti (1964), and Stix (1962). To be specific, the expressions for the MHD group velocities are

$$A_z^* = \cos(\theta + \delta)C_s + \frac{(a^2b^2 \sin\theta)(\cos\theta)\sin(\theta + \delta)}{C_s C} \quad (3.4)$$

and

$$A_r^* = \sin(\theta + \delta)C_s - \frac{(a^2b^2 \sin\theta)(\cos\theta)\cos(\theta + \delta)}{C_s C} \quad (3.5)$$

for the slow mode;

$$A_z = \cos(\theta + \delta)C_f - \frac{(a^2b^2 \sin\theta)(\cos\theta)\sin(\theta + \delta)}{C_f C} \quad (3.6)$$

and

$$A_r = \sin(\theta + \delta)C_f + \frac{(a^2b^2 \sin\theta)(\cos\theta)\cos(\theta + \delta)}{C_f C} \quad (3.7)$$

for the fast mode; and

$$A_z^t = \pm b \cos\delta \quad (3.8)$$

and

$$A_r^t = \pm b \sin\delta \quad (3.9)$$

for the transverse mode, where

$$C \equiv [(a^2 + b^2)^2 - 4a^2b^2 \cos^2\theta]^{1/2}, \quad (3.10)$$

θ is the angle between the wave vector $\boldsymbol{k}$ and the ambient magnetic field $\boldsymbol{B}$ (see Fig. 1), and (generalizing slightly) δ is the angle between $\boldsymbol{B}$ and the z-axis.

The general characteristic theory is presented by Courant and Hilbert (1962). The key property of the two-dimensional second-order partial differential equations (pde's) of the type (2.6)–(2.13) is that there exists a set of special coordinates (the characteristic coordinates) which allows one to reduce the number of independent variables of the equations by expressing them on a set of special surfaces called the characteristic surfaces. The analog of this in one-dimensional flow is that the pde's reduce to ordinary differential equations along characteristic lines. In contrast to the two characteristic lines in the one-dimensional flow case, there is an infinite number of characteristic surfaces in two-dimensional flow. The envelope of the family of the characteristic surfaces forms the characteristic cone in (t, r, z)-space (see Fig. 1).

Physically, the characteristic cone can be obtained from the linearized equations for small-amplitude perturbations. The tangent line between the characteristic surface and the characteristic cone is called the bicharacteristic. For a stationary, homogeneous background, the characteristic cones have a regular shape in (t, r, z)-space, and are determined by the unperturbed background state. In this simple case, the speeds with which the wavefront of the characteristic cones evolves in time are given by expressions (3.4)–(3.9). For a static, inhomogeneous background, the characteristic cones have an irregular shape in (t, r, z)-space, and are constructed according to the local properties of the background state. In this case, the speeds with which the wavefront of the characteristic cones evolves in time are given by expressions (3.4)–(3.9) as determined by the local properties. In the presence of a background flow, the characteristic cones are superposed onto the background flow. Thus, in addition to modifying the background properties, the background flow distorts the wavefront of the characteristic cones, and the shapes of the characteristic cones will depend on the solution to pde's (2.6)–(2.12).

We now apply the characteristic method to solve the pde's for nonlinear MHD motions in an inhomogeneous medium in the presence of a background flow. There are two important aspects involved. First, at each time step, the construction of characteristic cones has meaning only locally and differentially. Second, the pde's must be expressed along the characteristic cones so that the physical variables at the new time step are related to those at the old time step along the bicharacteristics. The basic idea here is that, for sufficiently small time steps, local characteristic cones can be constructed for nonlinear MHD motions in an inhomogeneous medium from the finite difference form of the equations along the bicharacteristics. The values of the physical variables at the new time step can then be obtained by numerical iteration. We see immediately that because of nonlinear motions and the inhomogeneous background, the maximum allowable time step for convergence is different at different spatial points and at different times. We must choose the minimum step size at each time to advance the calculation to the next time step so that convergence and stability can be guaranteed.

The local bicharacteristics along the characteristic cones for the various modes are defined by the local tangent vector $\tau \equiv (dr, dz, dt)$, where dr and dz are given by

$$dr = (u + A_r^*)dt \quad (3.11)$$

and

$$dz = (v + A_z^*)dt \quad (3.12)$$

for the slow mode;

$$dr = (u + A_r)dt \quad (3.13)$$

and

$$dz = (u + A_z)dt \quad (3.14)$$

for the fast mode;

$$dr = (u + A_r^t)dt \quad (3.15)$$

and

$$dz = (v + A_z^t)dt \quad (3.16)$$

for the transverse Alfvén mode. The quantities u and v are the r- and z-component background flow velocities, respectively, A_r^*, A_z^*, A_r, A_z, A_r^t, and A_z^t are defined by equations (3.4)–(3.9), and

$$dr = udt \quad (3.17)$$

and

$$dz = vdt \quad (3.18)$$

define the orientation of the axis of the characteristic cone [i.e., the local tangent vector to the fluid line in (t, r, z)-space.

The macroscopic disturbance patterns are distorted by the flows and by the inhomogeneity of the background variables.

Hence, after some time, it may be hard to distinguish previously distinct modes. However, in principle, if the macroscopic disturbance patterns are known at one time, they can be constructed for later times by using equations (3.11)–(3.16).

We are now in a position to express the MHD equations (2.6)–(2.13) on the characteristic cone. This will be done in the next section.

IV. METHOD OF BICHARACTERISTICS

We want to express equations (2.6)–(2.13) along the fast cone and the fluid line for an axisymmetric system, with $v_\phi = 0$ and $B_\phi = 0$. In a frame moving with the speed of disturbance of the fast mode, the time rate of change of any physical variable h is

$$\frac{dh}{dt} = \frac{\partial h}{\partial t} + (u + A_r)\frac{\partial h}{\partial r} + (v + A_z)\frac{\partial h}{\partial z}. \tag{4.1}$$

In a frame moving with the fluid line, the time rate of change of any physical variable h is

$$\frac{Dh}{Dt} = \frac{\partial h}{\partial t} + u\frac{\partial h}{\partial r} + v\frac{\partial h}{\partial z}. \tag{4.2}$$

Thus, along the fast cone, the MHD equations (2.6), (2.7), (2.10), (2.11), and (2.13) can be written as

$$\frac{du}{dt} + \frac{1}{\rho}\frac{\partial p}{\partial r} - \frac{B_z}{4\pi\rho}\frac{\partial B_r}{\partial z} + \frac{B_z}{4\pi\rho}\frac{\partial B_z}{\partial r} - A_r\frac{\partial u}{\partial r} - A_z\frac{\partial u}{\partial z} = 0, \tag{4.3}$$

$$\frac{dv}{dt} + \frac{1}{\rho}\frac{\partial p}{\partial z} + \frac{B_r}{4\pi\rho}\frac{\partial B_r}{\partial z} - \frac{B_r}{4\pi\rho}\frac{\partial B_z}{\partial r} - A_r\frac{\partial v}{\partial r} - A_z\frac{\partial v}{\partial z} = 0, \tag{4.4}$$

$$\frac{dB_r}{dt} + \frac{uB_r}{r} + B_r\frac{\partial v}{\partial z} - B_z\frac{\partial u}{\partial z} - A_r\frac{\partial B_r}{\partial r} - A_z\frac{\partial B_r}{\partial z} = 0, \tag{4.5}$$

$$\frac{dB_z}{dt} + \frac{uB_z}{r} - B_r\frac{\partial v}{\partial r} + B_z\frac{\partial u}{\partial r} - A_r\frac{\partial B_z}{\partial r} - A_z\frac{\partial B_z}{\partial z} = 0, \tag{4.6}$$

$$\frac{dp}{dt} + \rho a^2\left(\frac{\partial u}{\partial r} + \frac{\partial v}{\partial z} + \frac{u}{r}\right) - A_r\frac{\partial p}{\partial r} - A_z\frac{\partial p}{\partial z} = 0. \tag{4.7}$$

Along the fluid line, equation (2.9) is

$$\frac{D(p\rho^{-\gamma})}{Dt} = 0. \tag{4.8}$$

Combining equations (4.3), (4.4), and (4.7), we obtain

$$\frac{dp}{dt} + \rho A_r\frac{du}{dt} + \rho A_z\frac{dv}{dt} + \frac{(A_z B_r - A_r B_z)}{4\pi}\left(\frac{\partial B_r}{\partial z} - \frac{\partial B_z}{\partial r}\right) + \rho(a^2 - A_r^2)\frac{\partial u}{\partial r} + \rho(a^2 - A_z^2)\frac{\partial v}{\partial z} - \rho A_r A_z\left(\frac{\partial u}{\partial z} + \frac{\partial v}{\partial r}\right) + \frac{\rho a^2 u}{r} = 0. \tag{4.9}$$

Combining equations (4.3)–(4.6), we obtain

$$\rho A_z\frac{dB_r}{dt} - \rho A_r\frac{dB_z}{dt} - B_z\rho\frac{du}{dt} + B_r\rho\frac{dv}{dt} + \left(\frac{B_r^2 + B_z^2}{4\pi} - \rho A_z^2\right)\left(\frac{\partial B_r}{\partial z}\right) - \left(\frac{B_r^2 + B_z^2}{4\pi} - \rho A_r^2\right)\left(\frac{\partial B_z}{\partial r}\right) + B_r\left(\frac{\partial p}{\partial z}\right) - B_z\left(\frac{\partial p}{\partial r}\right) - \rho A_z A_r\left(\frac{\partial B_r}{\partial r} - \frac{\partial B_z}{\partial z}\right) + \frac{\rho u}{r}(A_z B_r - A_r B_z) = 0. \tag{4.10}$$

Along the fluid line, equation (4.7) is

$$\frac{Dp}{Dt} + \rho a^2\left(\frac{\partial u}{\partial r} + \frac{\partial v}{\partial z} + \frac{u}{r}\right) = 0. \tag{4.11}$$

We approximate the differential equations (4.9), (4.10), and (4.11) by the following finite difference scheme. The time derivative of any physical variable along the fast characteristic cone dh/dt or along the fluid line, Dh/Dt, is approximated by $(h_0 - h_n)/\Delta t$, where h represents any physical variable, subscript zero indicates that the variable h is evaluated at the point P_0 at the new time surface (see Fig. 2), and subscript n indicates that the variable h is evaluated at the points P_n at the old time surface, corresponding to different directions of the bicharacteristics along the characteristic cone or corresponding to the direction of the fluid line. The coefficients of the time derivatives of the physical variables and the terms not involving the time derivatives d/dt are approximated by the arithmetic means of their values at the new and old time surfaces. In so doing, the spatial derivatives of the unknown physical variables at the new time surface are needed. We then choose bicharacteristics in different directions along the characteristic cone to obtain enough equations so that these unknown spatial derivatives at the new time surface can be eliminated by appropriate linear combinations of the equations along the different bicharacteristics. Physical variables and their spatial derivatives at the old time surface are interpolated by a two-dimensional cubic spline scheme (Stefanik *et al.* 1984; Späth 1973). The detailed numerical procedure is described in the next section.

V. NUMERICAL PROCEDURE

Following the basic idea of the method of bicharacteristics described in § IV and retaining the notation developed there, equation (4.9) can be written as

$$p_0 - B^f_{zn}u_0 + B^f_{rn}v_0 - T^f_n = -\frac{W^f_{0,n}\Delta t}{2}, \tag{5.1}$$

where

$$B^f_{zn} \equiv -(\rho_0 A_{r0,n} + \rho_n A_{rn})/2, \tag{5.2}$$

$$B^f_{rn} \equiv (\rho_0 A_{z0,n} + \rho_n A_{zn})/2, \tag{5.3}$$

$$W^f_{0,n} \equiv \frac{(A_{z0,n}B_{r0} - A_{r0,n}B_{z0})}{4\pi}\left[\left(\frac{\partial B_r}{\partial z}\right)_0 - \left(\frac{\partial B_z}{\partial r}\right)_0\right] + \rho_0(a_0^2 - A_{r0,n}^2)\left(\frac{\partial u}{\partial r}\right)_0 + \rho_0(a_0^2 - A_{z0,n}^2)\left(\frac{\partial v}{\partial z}\right)_0 - \rho_0 A_{r0,n}A_{z0,n}\left[\left(\frac{\partial u}{\partial z}\right)_0 + \left(\frac{\partial v}{\partial r}\right)_0\right] + \frac{\rho_0 a_0^2 u_0}{r_0}, \tag{5.4}$$

$$W^f_n \equiv \frac{(A_{zn}B_{rn} - A_{rn}B_{zn})}{4\pi}\left[\left(\frac{\partial B_r}{\partial z}\right)_n - \left(\frac{\partial B_z}{\partial r}\right)_n\right] + \rho_n(a_n^2 - A_{rn}^2)\left(\frac{\partial u}{\partial r}\right)_n + \rho_n(a_n^2 - A_{zn}^2)\left(\frac{\partial v}{\partial z}\right)_n - \rho_n A_{rn}A_{zn}\left[\left(\frac{\partial u}{\partial z}\right)_n + \left(\frac{\partial v}{\partial r}\right)_n\right] + \frac{\rho_n a_n^2 u_n}{r_n}, \tag{5.5}$$

and

$$T^f_n \equiv -B^f_{zn}u_n + B^f_{rn}v_n - W^f_n\frac{\Delta t}{2} + p_n. \tag{5.6}$$

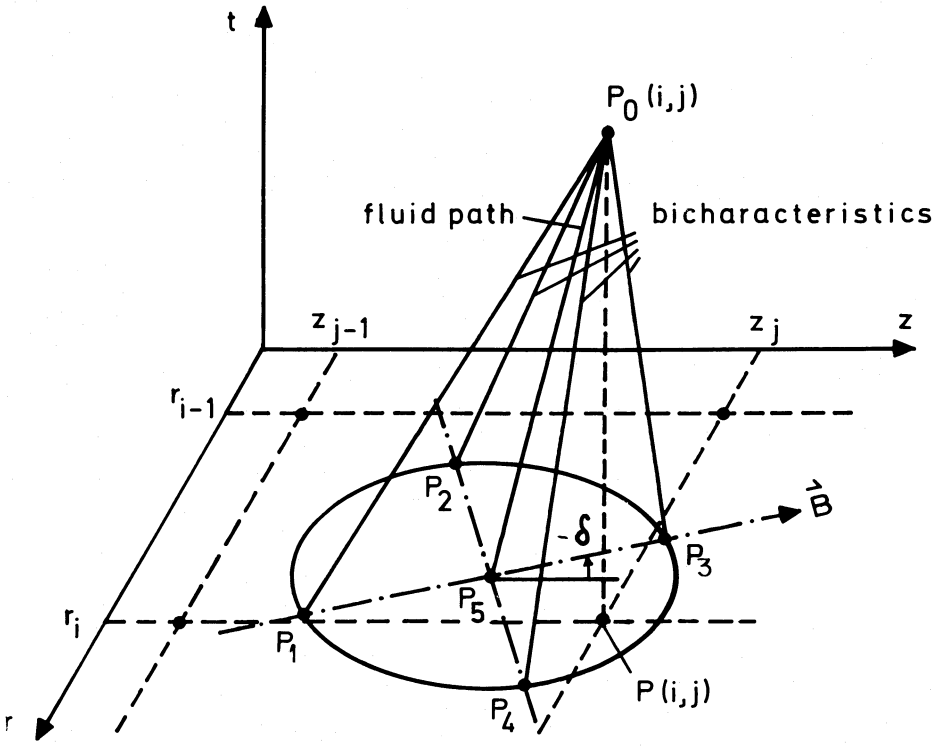

FIG. 2.—The local fast cone and the fluid path in the neighborhood of a grid point $P(i, j)$. $P_0(i, j)$ is the same spatial point at the next time step

The directions $n = 1, 2, 3$, and 4 are chosen corresponding to $\theta = 0, \pi/2, \pi$, and $3\pi/2$ (see Fig. 2). We use n to label the corresponding bicharacteristics. From the four equations (5.1) (for $n = 1, 2, 3$, and 4), we obtain

$$-(B_{z1}^f - B_{z3}^f)u_0 + (B_{r1}^f - B_{r3}^f)v_0 - (T_1^f - T_3^f) = -\frac{(A_{z0,1}B_{r0} - A_{r0,1}B_{z0})}{2\pi}\left[\left(\frac{\partial B_r}{\partial z}\right)_0 - \left(\frac{\partial B_z}{\partial r}\right)_0\right]\frac{\Delta t}{2}, \quad (5.7)$$

and

$$-(B_{z2}^f - B_{z4}^f)u_0 + (B_{r2}^f - B_{r4}^f)v_0 - (T_2^f - T_4^f) = -\frac{(A_{z0,2}B_{r0} - A_{r0,2}B_{z0})}{2\pi}\left[\left(\frac{\partial B_r}{\partial z}\right)_0 - \left(\frac{\partial B_z}{\partial r}\right)_0\right]\frac{\Delta t}{2}. \quad (5.8)$$

Here we have used that $A_{r0,3} = -A_{r0,1}$, $A_{z0,3} = -A_{z0,1}$, $A_{r0,4} = -A_{r0,2}$, and $A_{z0,4} = -A_{z0,2}$. Equations (5.7) and (5.8) contain $(\partial B_r/\partial z)_0$ and $(\partial B_z/\partial r)_0$, which are unknowns introduced by our approximation scheme. Differencing equation (4.5) along the four bicharacteristics and subtracting, one obtains

$$(A_{r0,1} - A_{r0,3})\left(\frac{\partial B_r}{\partial r}\right)_0\frac{\Delta t}{2} + (A_{z0,1} - A_{z0,3})\left(\frac{\partial B_r}{\partial z}\right)_0\frac{\Delta t}{2} = -(B_{r1} - B_{r3}) + \frac{\Delta t}{2}(Y_1 - Y_3), \quad (5.9)$$

and

$$(A_{r0,2} - A_{r0,4})\left(\frac{\partial B_r}{\partial r}\right)_0\frac{\Delta t}{2} + (A_{z0,2} - A_{z0,4})\left(\frac{\partial B_r}{\partial z}\right)_0\frac{\Delta t}{2} = -(B_{r2} - B_{r4}) + \frac{\Delta t}{2}(Y_2 - Y_4), \quad (5.10)$$

where

$$Y_n \equiv \frac{u_n B_{rn}}{r_n} + B_{rn}\left(\frac{\partial v}{\partial z}\right)_n - B_{zn}\left(\frac{\partial u}{\partial z}\right)_n - A_{rn}\left(\frac{\partial B_r}{\partial r}\right)_n - A_{zn}\left(\frac{\partial B_r}{\partial z}\right)_n. \quad (5.11)$$

Solving equations (5.9) and (5.10), one obtains

$$\left(\frac{\partial B_r}{\partial z}\right)_0\frac{\Delta t}{2} = \left\{A_{r0,2}\left[-(B_{r1} - B_{r3}) + \frac{\Delta t}{2}(Y_1 - Y_3)\right] - A_{r0,1}\left[-(B_{r2} - B_{r4}) + \frac{\Delta t}{2}(Y_2 - Y_4)\right]\right\}\Big/ 2[A_{r0,2}A_{z0,1} - A_{z0,2}A_{r0,1}]. \quad (5.12)$$

Similarly, differencing equation (4.6) along the four bicharacteristics and subtracting, one obtains

$$(A_{r0,1} - A_{r0,3})\left(\frac{\partial B_z}{\partial r}\right)_0\frac{\Delta t}{2} + (A_{z0,1} - A_{z0,3})\left(\frac{\partial B_z}{\partial z}\right)_0\frac{\Delta t}{2} = -(B_{z1} - B_{z3}) + \frac{\Delta t}{2}(X_1 - X_3), \quad (5.13)$$

and

$$(A_{r0,2} - A_{r0,4})\left(\frac{\partial B_z}{\partial r}\right)_0\frac{\Delta t}{2} + (A_{z0,2} - A_{z0,4})\left(\frac{\partial B_z}{\partial z}\right)_0\frac{\Delta t}{2} = -(B_{z2} - B_{z4}) + \frac{\Delta t}{2}(X_2 - X_4), \quad (5.14)$$

where

$$X_n \equiv \frac{u_n B_{zn}}{r_n} - B_{rn}\left(\frac{\partial v}{\partial r}\right)_n + B_{zn}\left(\frac{\partial u}{\partial r}\right)_n - A_{rn}\left(\frac{\partial B_z}{\partial r}\right)_n - A_{zn}\left(\frac{\partial B_z}{\partial z}\right)_n . \quad (5.15)$$

From equations (5.13) and (5.14), one obtains

$$\left(\frac{\partial B_z}{\partial r}\right)_0 \frac{\Delta t}{2} = \left\{A_{z0,1}\left[-(B_{z2} - B_{z4}) + \frac{\Delta t}{2}(X_2 - X_4)\right] - A_{z0,2}\left[-(B_{z1} - B_{z3}) + \frac{\Delta t}{2}(X_1 - X_3)\right]\right\} \Big/ 2[A_{r0,2} A_{z0,1} - A_{z0,2} A_{r0,1}] . \quad (5.16)$$

Combining equations (5.12) and (5.16), we have

$$\left[\left(\frac{\partial B_r}{\partial z}\right)_0 - \left(\frac{\partial B_z}{\partial r}\right)_0\right]\frac{\Delta t}{2} = \left\{A_{r0,2}\left[-(B_{r1} - B_{r3}) + \frac{\Delta t}{2}(Y_1 - Y_3)\right] - A_{r0,1}\left[-(B_{r2} - B_{r4}) + \frac{\Delta t}{2}(Y_2 - Y_4)\right] + A_{z0,2}\left[-(B_{z1} - B_{z3}) + \frac{\Delta t}{2}(X_1 - X_3)\right] - A_{z0,1}\left[-(B_{z2} - B_{z4}) + \frac{\Delta t}{2}(X_2 - X_4)\right]\right\} \Big/ 2[A_{r0,2} A_{z0,1} - A_{z0,2} A_{r0,1}] . \quad (5.17)$$

Substituting equation (5.17) into equations (5.7) and (5.8), u_0 and v_0 can be solved for by numerical iteration.

With the same numerical approximations, the finite difference form of equation (4.10) can be written along the four bicharacteristics as

$$B^f_{rn} B_{r0} + B^f_{zn} B_{z0} + U_n u_0 + V_n v_0 - R^f_n = -G^f_{0,n}\frac{\Delta t}{2} , \quad (5.18)$$

where

$$U_n \equiv -(B_{z0}\rho_0 + B_{zn}\rho_n)/2 , \quad (5.19)$$

$$V_n \equiv (B_{r0}\rho_0 + B_{rn}\rho_n)/2 , \quad (5.20)$$

$$G^f_n \equiv \left(\frac{B^2_{rn} + B^2_{zn}}{4\pi} - \rho_n A^2_{zn}\right)\left(\frac{\partial B_r}{\partial z}\right)_n - \left(\frac{B^2_{rn} + B^2_{zn}}{4\pi} - \rho_n A^2_{rn}\right) \times \left(\frac{\partial B_z}{\partial r}\right)_n + B_{rn}\left(\frac{\partial p}{\partial z}\right)_n - B_{zn}\left(\frac{\partial p}{\partial r}\right)_n - \rho_n A_{zn} A_{rn}\left[\left(\frac{\partial B_r}{\partial r}\right)_n - \left(\frac{\partial B_z}{\partial z}\right)_n\right] + \frac{\rho_n u_n}{r_n}(A_{zn} B_{rn} - A_{rn} B_{zn}) , \quad (5.21)$$

$$R^f_n \equiv B^f_{rn} B_{rn} + B^f_{zn} B_{zn} + U_n u_n + V_n v_n - G^f_n \frac{\Delta t}{2} , \quad (5.22)$$

and

$$G^f_{0,n} \equiv \left(\frac{B^2_{r0} + B^2_{z0}}{4\pi} - \rho_0 A^2_{z0,n}\right)\left(\frac{\partial B_r}{\partial z}\right)_0 - \left(\frac{B^2_{r0} + B^2_{z0}}{4\pi} - \rho_0 A^2_{r0,n}\right)\left(\frac{\partial B_z}{\partial r}\right)_0 + B_{r0}\left(\frac{\partial p}{\partial z}\right)_0 - B_{z0}\left(\frac{\partial p}{\partial r}\right)_0 - \rho_0 A_{z0,n} A_{r0,n}\left[\left(\frac{\partial B_r}{\partial r}\right)_0 - \left(\frac{\partial B_z}{\partial z}\right)_0\right] + \frac{\rho_0 u_0}{r_0}(A_{z0,n} B_{r0} - A_{r0,n} B_{z0}) . \quad (5.23)$$

From the four equations (5.18), corresponding to $n = 1, 2, 3$, and 4, one obtains

$$(B^f_{r1} - B^f_{r3})B_{r0} + (B^f_{z1} - B^f_{z3})B_{z0} = (R^f_1 - R^f_3) - (U_1 - U_3)u_0 - (V_1 - V_3)v_0 - (G^f_{0,1} - G^f_{0,3})\frac{\Delta t}{2} , \quad (5.24)$$

and

$$(B^f_{r2} - B^f_{r4})B_{r0} + (B^f_{z2} - B^f_{z4})B_{z0} = (R^f_2 - R^f_4) - (U_2 - U_4)u_0 - (V_2 - V_4)v_0 - (G^f_{0,2} - G^f_{0,4})\frac{\Delta t}{2} . \quad (5.25)$$

From equations (5.24) and (5.25) with u_0 and v_0 given by equations (5.7) and (5.8), B_{r0} and B_{z0} can be solved for by numerical iteration.

In similar fashion, the finite difference form of equation (4.11) is written as

$$p_0 = T^f_5 \Big/ \left\{1 + \gamma\left[\left(\frac{\partial u}{\partial r}\right)_0 + \left(\frac{\partial v}{\partial z}\right)_0 + \frac{u_0}{r_0}\right]\frac{\Delta t}{2}\right\} , \quad (5.26)$$

where

$$T^f_5 \equiv p_5 - \rho_5 a^2_5\left[\left(\frac{\partial u}{\partial r}\right)_5 + \left(\frac{\partial v}{\partial z}\right)_5 + \left(\frac{u}{r}\right)_5\right]\frac{\Delta t}{2} . \quad (5.27)$$

Subscript "5" indicates that the quantities are those at the point P_5, corresponding to the intersection of the fluid line and the old time surface (see Fig. 2).

In equation (5.26), $(\partial u/\partial r)_0$ and $(\partial v/\partial z)_0$ are two unknowns. Differencing equation (4.3) along the four bicharacteristics, we write

$$u_0 - u_n + Z_n\frac{\Delta t}{2} + \left[\frac{1}{\rho_0}\left(\frac{\partial p}{\partial r}\right)_0 - \frac{B_{z0}}{4\pi\rho_0}\left(\frac{\partial B_r}{\partial z}\right)_0 + \frac{B_{z0}}{4\pi\rho_0}\left(\frac{\partial B_z}{\partial r}\right)_0\right]\frac{\Delta t}{2} = A_{r0,n}\left(\frac{\partial u}{\partial r}\right)_0\frac{\Delta t}{2} + A_{z0,n}\left(\frac{\partial u}{\partial z}\right)_0\frac{\Delta t}{2} , \quad (5.28)$$

where

$$Z_n \equiv \frac{1}{\rho_n}\left(\frac{\partial p}{\partial r}\right)_n - \frac{B_{zn}}{4\pi\rho_n}\left(\frac{\partial B_r}{\partial z}\right)_n + \frac{B_{zn}}{4\pi\rho_n}\left(\frac{\partial B_z}{\partial r}\right)_n - A_{rn}\left(\frac{\partial u}{\partial r}\right)_n - A_{zn}\left(\frac{\partial u}{\partial z}\right)_n . \quad (5.29)$$

From the four equations (5.28) (for $n = 1$, 2, 3, and 4), one obtains

$$2A_{r0,1}\left(\frac{\partial u}{\partial r}\right)_0 \frac{\Delta t}{2} + 2A_{z0,1}\left(\frac{\partial u}{\partial z}\right)_0 \frac{\Delta t}{2} = -(u_1 - u_3) + \frac{\Delta t}{2}(Z_1 - Z_3), \quad (5.30)$$

and

$$2A_{r0,2}\left(\frac{\partial u}{\partial r}\right)_0 \frac{\Delta t}{2} + 2A_{z0,2}\left(\frac{\partial u}{\partial z}\right)_0 \frac{\Delta t}{2} = -(u_2 - u_4) + \frac{\Delta t}{2}(Z_2 - Z_4). \quad (5.31)$$

Solving equations (5.30) and (5.31), one obtains

$$\left(\frac{\partial u}{\partial r}\right)_0 \frac{\Delta t}{2} = \left\{A_{z0,2}\left[-(u_1 - u_3) + \frac{\Delta t}{2}(Z_1 - Z_3)\right] - A_{z0,1}\left[-(u_2 - u_4) + \frac{\Delta t}{2}(Z_2 - Z_4)\right]\right\} \Big/ 2(A_{r0,1}A_{z0,2} - A_{z0,1}A_{r0,2}). \quad (5.32)$$

Similarly, differencing equation (4.4) along the four bicharacteristics, we have

$$v_0 - v_n + S_n \frac{\Delta t}{2} + \left[\frac{1}{\rho_0}\left(\frac{\partial p}{\partial z}\right)_0 + \frac{B_{r0}}{4\pi\rho_0}\left(\frac{\partial B_r}{\partial z}\right)_0 - \frac{B_{r0}}{4\pi\rho_0}\left(\frac{\partial B_z}{\partial r}\right)_0\right]\frac{\Delta t}{2} = A_{r0,n}\left(\frac{\partial v}{\partial r}\right)_0 \frac{\Delta t}{2} + A_{z0,n}\left(\frac{\partial v}{\partial z}\right)_0 \frac{\Delta t}{2}, \quad (5.33)$$

where

$$S_n \equiv \frac{1}{\rho_n}\left(\frac{\partial p}{\partial z}\right)_n + \frac{B_{rn}}{4\pi\rho_n}\left(\frac{\partial B_r}{\partial z}\right)_n - \frac{B_{rn}}{4\pi\rho_n}\left(\frac{\partial B_z}{\partial r}\right)_n - A_{rn}\left(\frac{\partial v}{\partial r}\right)_n - A_{zn}\left(\frac{\partial v}{\partial z}\right)_n. \quad (5.34)$$

From the four equations (5.33) (for $n = 1$, 2, 3, and 4), one obtains

$$2A_{r0,1}\left(\frac{\partial v}{\partial r}\right)_0 \frac{\Delta t}{2} + 2A_{z0,1}\left(\frac{\partial v}{\partial z}\right)_0 \frac{\Delta t}{2} = -(v_1 - v_3) + \frac{\Delta t}{2}(S_1 - S_3), \quad (5.35)$$

and

$$2A_{r0,2}\left(\frac{\partial v}{\partial r}\right)_0 \frac{\Delta t}{2} + 2A_{z0,2}\left(\frac{\partial v}{\partial z}\right)_0 \frac{\Delta t}{2} = -(v_2 - v_4) + \frac{\Delta t}{2}(S_2 - S_4). \quad (5.36)$$

Solving equations (5.35) and (5.36), one obtains

$$\left(\frac{\partial v}{\partial z}\right)_0 \frac{\Delta t}{2} = \left\{A_{r0,1}\left[-(v_2 - v_4) + \frac{\Delta t}{2}(S_2 - S_4)\right] - A_{r0,2}\left[-(v_1 - v_3) + \frac{\Delta t}{2}(S_1 - S_3)\right]\right\} \Big/ 2(A_{r0,1}A_{z0,2} - A_{z0,1}A_{r0,2}). \quad (5.37)$$

The quantity p_0 is then obtained by substituting equations (5.32) and (5.37) into equation (5.26).

From equation (4.8) along the fluid line, the density is given by

$$\rho_0 = \rho_5\left(\frac{p_0}{p_5}\right)^{1/\gamma}. \quad (5.38)$$

In summary, we use equations (5.7), (5.8), (5.17), (5.24), (5.26), (5.32), (5.37), and (5.38) to solve for u_0, v_0, B_{r0}, B_{z0}, p_0, and ρ_0 in terms of the variables at points P_n, corresponding to $n = 1$, 2, 3, 4, and 5, by numerical iteration. The expressions relating the coordinates of P_0 to those at P_n are obtained from equations (3.13), (3.14), (3.17), and (3.18) for the bicharacteristics and the fluid path. In finite difference form, we write

$$r_n = r_0 - \frac{\Delta t}{2}(u_0 + u_n + A_{r0,n} + A_{rn}), \quad (5.39)$$

and

$$z_n = z_0 - \frac{\Delta t}{2}(v_0 + v_n + A_{z0,n} + A_{zn}), \quad (5.40)$$

where $n = 1$, 2, 3, and 4 for the bicharacteristics on the fast cone and

$$r_5 = r_0 - \frac{\Delta t}{2}(u_0 + u_5) \quad (5.41)$$

and

$$z_5 = z_0 - \frac{\Delta t}{2}(v_0 + v_5) \quad (5.42)$$

for the fluid path. At present, we neglect the winding of the bicharacteristics along the fast cone due to the flows. In the MHD case, the Courant time step is defined by the grid size divided by $C_f(\theta = \pi/2)$ according to equation (3.1).

The numerical iteration procedure to solve for the physical variables at point $P_0(i, j)$ is as follows (see Fig. 2). We first use the initial data at the grid point $P(i, j)$ to find rough estimates of the positions r_n and z_n ($n = 1$, 2, 3, 4, and 5) by equations (5.39)–(5.42) without arithmetic averages. With a two-dimensional cubic spline interpolation in space (Stefanik *et al.* 1984), the physical variables and their derivatives are interpolated at the points P_n from the known data at the grid points $P(i, j)$. Using equations (5.7), (5.8), (5.17), (5.24)–(5.26), (5.32), (5.37), and (5.38), the new physical variables u_0, v_0, B_{r0}, B_{z0}, p_0, and ρ_0 are then computed for the point $P_0(i, j)$. We then continue this iteration until the results converge.

In general, we do not have theoretical guidance as to the convergence of the numerical iteration scheme for nonlinear equations such as those discussed here. The problem is that the domain of convergence in the function space defined by the dependent variables is highly sensitive to both the initial estimates of the dependent variables and the numerical iteration scheme, and that the domains of convergence vary at different points due to the nonlinearity of the equations. We do know that reducing the time step will, in general, increase the domains of convergence, and that by linearizing the nonlinear equations, we may in principle use the Von Neumann condition (Richtmyer 1957; Shin and Kot 1978) to find the maximum time step for convergence for a given grid size. However, because we use a complicated cubic spline interpolation scheme at each iterative step, such an explicit analytical analysis is formidable even in linear regime, and we have

instead checked for convergence by considering the numerical results themselves. For our test examples, the numerical iteration scheme described above in fact converges well, and highly accurate results are obtained for the given time step, spatial grid size, and the physical parameters; for example, we typically converged within 3–4 cycles for the magnetized expanding ball problem discussed below.

VI. THE TREATMENT OF BOUNDARY CONDITIONS

The calculation of the physical variables at the interior points can be carried out by using the equations prescribed in § V. In this section, we focus on the treatment of axial and boundary points because the treatment of the boundary points depends on the specific boundary conditions. The following treatment of the boundary points is pertinent to the problem of the standing MHD waves described in §§ VII*a*, *c*; the problem of the nonlinear, self-similar expansion of a magnetized plasma ball described in § VII*b* has no physical boundary.

a) The Axial Points

Our coordinate system is chosen such that the background magnetic field $\boldsymbol{B}_0$ is parallel to the axis of symmetry. On the axis of symmetry, bicharacteristic number 2 is missing (see Fig. 3). Two physical variables are known from the geometric symmetry condition,

$$u = 0 , \tag{6.1}$$

and

$$B_r = 0 ; \tag{6.2}$$

that is, the magnetic field $\boldsymbol{B}$ is always parallel to the axis of symmetry. With the conditions (6.1) and (6.2) on the axis, it follows that

$$\frac{\partial u}{\partial z} = 0 , \tag{6.3}$$

and

$$\frac{\partial B_r}{\partial z} = 0 . \tag{6.4}$$

On the axis, equation (2.6) reduces to

$$\frac{\partial}{\partial r}\left(p + \frac{B_z^2}{8\pi}\right) = 0 , \tag{6.5}$$

and u/r reduces to $\partial u/\partial r$. Along the fluid line, the density is given by

$$\rho_0 = \rho_5\left(\frac{p_0}{p_5}\right)^{1/\gamma} . \tag{6.6}$$

From equation (5.7), one obtains

$$v_0 = (T_1^f - T_3^f)/(B_{r1}^f - B_{r3}^f) , \tag{6.7}$$

where we have used the fact that the cross product of the group velocity in the direction of the magnetic field and the magnetic field is equal to zero.

With $n = 4$ in equation (5.28) and using equations (6.1), (6.3)–(6.5), one obtains

$$\left(\frac{\partial u}{\partial r}\right)_0 \frac{\Delta t}{2} = \left(-u_4 + \frac{\Delta t}{2} Z_4\right) \Big/ A_{r0,4} , \tag{6.8}$$

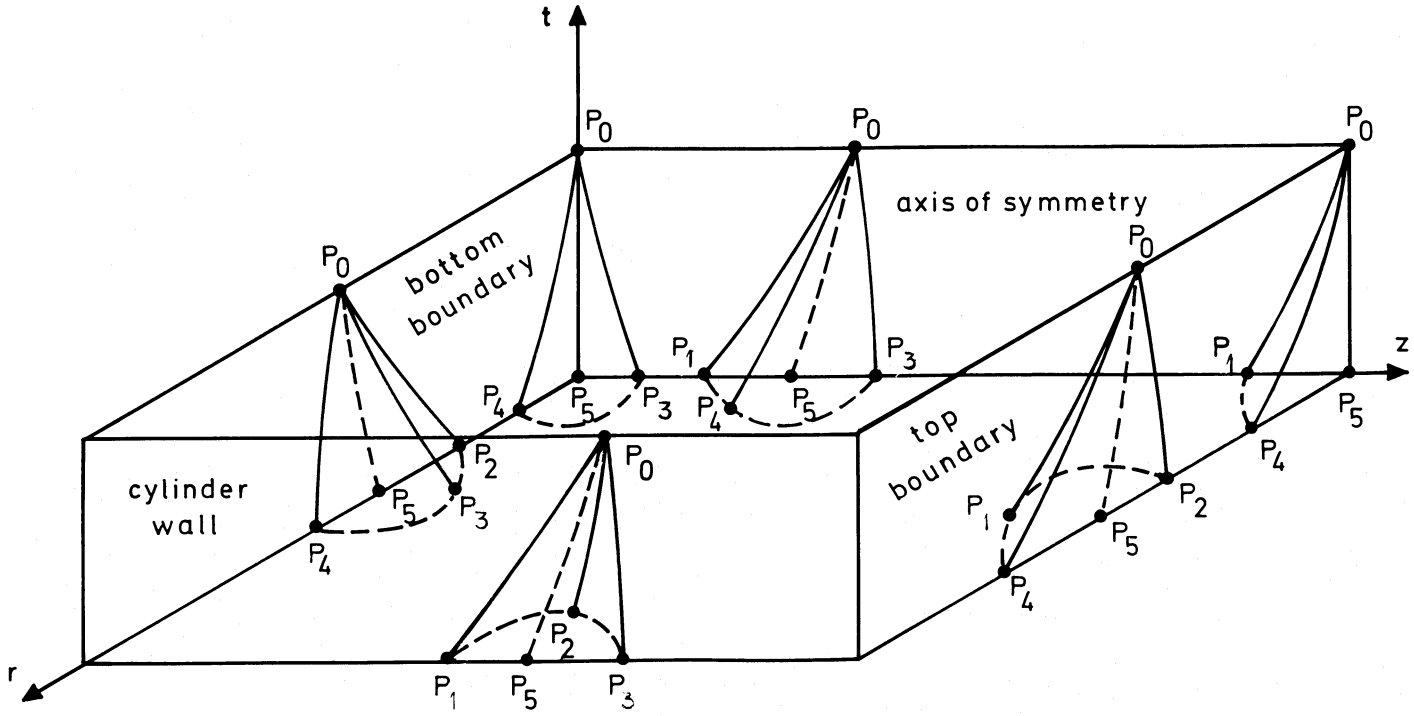

FIG. 3.—Geometry of the fast cones at the boundaries and at the corner points

and with $A_{r0,1} = 0$, equation (5.35) gives

$$\left(\frac{\partial v}{\partial z}\right)_0 \frac{\Delta t}{2} = \left[-(v_1 - v_3) + \frac{\Delta t}{2}(S_1 - S_3)\right] \Big/ 2A_{z0,1} . \quad (6.9)$$

We then substitute equations (6.8) and (6.9) into equation (5.26) and use $u_0/r_0 = (\partial u/\partial r)_0$ to solve for the pressure p_0. Along the fluid line, equation (2.11) is

$$\frac{DB_z}{Dt} + \left(\frac{uB_z}{r} - B_r \frac{\partial v}{\partial r} + B_z \frac{\partial u}{\partial r}\right) = 0 . \quad (6.10)$$

Using $u/r = \partial u/\partial r$ and the fact that the fluid path remains on the axis of symmetry, the finite difference form of equation (6.10) can be written as

$$B_{z0} = B_{z5}\left[1 - \left(\frac{\partial u}{\partial r}\right)_5 \Delta t\right] \Big/ \left[1 + \left(\frac{\partial u}{\partial r}\right)_0 \Delta t\right] . \quad (6.11)$$

In summary, equations (6.7)–(6.9), (5.26), and (6.11) are used to solve for v_0, B_{z0}, p_0, and ρ_0 on the axis by numerical iteration.

b) *The Points on the Wall*

With rigid boundary conditions on the wall of the cylinder, the boundary treatment is similar to that for points on the axis except (i) $u/r_0 = 0$, and (ii) the bicharacteristic number 4 is missing (see Fig. 3). Thus equation (6.8) is modified by setting $n = 2$ in equation (5.28),

$$\left(\frac{\partial u}{\partial r}\right)_0 \frac{\Delta t}{2} = \left(-u_2 + \frac{\Delta t}{2} Z_2\right) \Big/ A_{r0,2} , \quad (6.12)$$

and using the fact that the fluid path remains on the wall, we have from equation (6.10)

$$B_{z0} = B_{z5}\left[1 - \left(\frac{\partial u}{\partial r}\right)_5 \frac{\Delta t}{2}\right] \Big/ \left[1 + \left(\frac{\partial u}{\partial r}\right)_0 \frac{\Delta t}{2}\right] . \quad (6.13)$$

In summary, equations (5.26), (6.6), (6.7), (6.9), (6.12), and (6.13) are used to solve for v_0, B_{z0}, p_0, and ρ_0 on the wall by numerical iteration.

c) *The Points on the Top*

With the boundary conditions on the top of the cylinder $z = L$ described in § VII*a*, we have the rigid wall condition

$$v = 0 , \quad (6.14)$$

and the condition

$$B_r = 0 . \quad (6.15)$$

From the boundary conditions (6.14) and (6.15), it follows that

$$\frac{\partial v}{\partial r} = 0 , \quad (6.16)$$

and

$$\frac{\partial B_r}{\partial r} = 0 . \quad (6.17)$$

From the divergence-free condition of the magnetic field, we must require

$$\frac{\partial B_z}{\partial z} = 0 \quad (6.18)$$

at the top of the cylinder. At the top, equation (2.7) reduces to

$$\frac{\partial p}{\partial z} = 0 . \quad (6.19)$$

Since the bicharacteristic number 3 is missing (see Fig. 3), we set $n = 1$ in equation (5.33) and obtain

$$\left(\frac{\partial v}{\partial z}\right)_0 \frac{\Delta t}{2} = \left(-v_1 + S_1 \frac{\Delta t}{2}\right) \Big/ A_{z0,1} . \quad (6.20)$$

Since $A_{z0,2} = 0$ at the top, equation (5.31) reduces to

$$\left(\frac{\partial u}{\partial r}\right)_0 \frac{\Delta t}{2} = \left[-(u_2 - u_4) + \frac{\Delta t}{2}(Z_2 - Z_4)\right] \Big/ 2A_{r0,2} . \quad (6.21)$$

Along the fluid line, the density is given by

$$\rho_0 = \rho_5 \left(\frac{p_0}{p_5}\right)^{1/\gamma} . \quad (6.22)$$

Substituting equations (6.20) and (6.21) into equation (5.26), the pressure is given by

$$p_0 = T_5^f \Big/ \left\{1 + \gamma\left[\left(\frac{\partial u}{\partial r}\right)_0 + \left(\frac{\partial v}{\partial z}\right)_0 + \frac{u_0}{r_0}\right]\frac{\Delta t}{2}\right\} . \quad (6.23)$$

At the top, differencing equation (6.10), we have

$$B_{z0} = \left\{B_{z5} - \left[\frac{u_5 B_{z5}}{r_5} - B_{r5}\left(\frac{\partial v}{\partial r}\right)_5 + B_{z5}\left(\frac{\partial u}{\partial r}\right)_5\right]\frac{\Delta t}{2}\right\} \Big/ \left\{1 + \left[\frac{u_0}{r_0} + \left(\frac{\partial u}{\partial r}\right)_0\right]\frac{\Delta t}{2}\right\} . \quad (6.24)$$

From equation (2.10) at the top, we have

$$\frac{\partial u}{\partial z} = 0 \quad (6.25)$$

since $B_z \neq 0$. By choosing $n = 1$, the finite difference form of equation (4.5) gives

$$\left(\frac{\partial B_r}{\partial z}\right)_0 \frac{\Delta t}{2} = \left(-B_{r1} + Y_1 \frac{\Delta t}{2}\right) \Big/ A_{z0,1} , \quad (6.26)$$

where Y_1 is defined by equation (5.11). Since $A_{z0,2} = 0$ and $A_{z0,4} = 0$ on the top, equation (5.14) reduces to

$$\left(\frac{\partial B_z}{\partial r}\right)_0 \frac{\Delta t}{2} = \left[-(B_{z2} - B_{z4}) + (X_2 - X_4)\frac{\Delta t}{2}\right] \Big/ (A_{r0,2} - A_{r0,4}) . \quad (6.27)$$

Substituting equations (6.26) and (6.27) into equation (5.8), we have

$$u_0 = \left\{T_2^f - T_4^f + \frac{A_{r0,2} B_{z0}}{2\pi}\left[\left(\frac{\partial B_r}{\partial z}\right)_0 - \left(\frac{\partial B_z}{\partial r}\right)_0\right]\frac{\Delta t}{2}\right\} \Big/ [-(B_{z2}^f - B_{z4}^f)] . \quad (6.28)$$

In summary, equations (6.20)–(6.24) and (6.26)–(6.28) are used to solve for ρ_0, p_0, B_{z0}, and u_0 by numerical iteration.

d) *The Points at the Bottom*

With the boundary conditions at the bottom of the cylinder $z = 0$ described in § VII*a*, the treatment is similar to that on

the top, except equation (6.20) is modified to read

$$\left(\frac{\partial v}{\partial z}\right)_0 \frac{\Delta t}{2} = \left(-v_3 + S_3 \frac{\Delta t}{2}\right) \Big/ A_{z0,3} , \tag{6.29}$$

and equation (6.26) is modified to read

$$\left(\frac{\partial B_r}{\partial z}\right)_0 \frac{\Delta t}{2} = \left(-B_{r3} + Y_3 \frac{\Delta t}{2}\right) \Big/ A_{z0,3} \tag{6.30}$$

by using the bicharacteristic number 3. Then equations (6.21)–(6.24) and (6.27)–(6.30) are used to solve for ρ_0, p_0, B_{z0}, and u_0 by numerical iteration.

e) *Points at Corners*

The coordinates of the four corner points are (I) ($r = 0$, $z = L$); (II) ($r = 0$, $z = 0$); (III) ($r = r_0$, $z = L$); (IV) ($r = r_0$, $z = 0$).

For corner point (I), the bicharacteristics number 2 and 3 are missing (see Fig. 3). We know from the rigid wall condition that

$$v = 0 , \tag{6.31}$$

and from the geometric symmetry condition that

$$u = 0 , \tag{6.32}$$

and

$$B_r = 0 . \tag{6.33}$$

It then follows that

$$\frac{\partial u}{\partial z} = 0 , \tag{6.34}$$

$$\frac{\partial B_r}{\partial z} = 0 , \tag{6.35}$$

$$\frac{\partial v}{\partial r} = 0 , \tag{6.36}$$

$$\frac{\partial B_r}{\partial r} = 0 , \tag{6.37}$$

where the last condition (6.37) is derived from the condition $B_r = 0$ on the top of the cylinder. Now u/r should be replaced by $\partial u/\partial r$. From equation (2.6), we have

$$\frac{\partial}{\partial r}\left(p + \frac{B_z^2}{8\pi}\right) = 0 . \tag{6.38}$$

From equation (2.7), we have

$$\frac{\partial p}{\partial z} = 0 . \tag{6.39}$$

From the divergence-free condition, we have

$$\frac{\partial B_z}{\partial z} = 0 . \tag{6.40}$$

Along the fluid line, the density is given by

$$\rho_0 = \rho_5 \left(\frac{p_0}{p_5}\right)^{1/\gamma} . \tag{6.41}$$

With $n = 4$ in equation (5.28) and $n = 1$ in equation (5.33), respectively, we have

$$\left(\frac{\partial u}{\partial r}\right)_0 \frac{\Delta t}{2} = \left(-u_4 + Z_4 \frac{\Delta t}{2}\right) \Big/ A_{r0,4} , \tag{6.42}$$

and

$$\left(\frac{\partial v}{\partial z}\right)_0 \frac{\Delta t}{2} = \left(-v_1 + S_1 \frac{\Delta t}{2}\right) \Big/ A_{z0,1} . \tag{6.43}$$

Substituting equations (6.42) and (6.43) into equation (5.26), we have

$$p_0 = T_5^f \Big/ \left\{1 + \gamma\left[2\left(\frac{\partial u}{\partial r}\right)_0 + \left(\frac{\partial v}{\partial z}\right)_0\right]\frac{\Delta t}{2}\right\} . \tag{6.44}$$

Thus, with equations (6.11) and (6.41)–(6.44), B_{z0}, p_0, and ρ_0 are solved for by numerical iteration.

Similarly, for corner point (II), the bicharacteristics number 1 and 2 are missing (see Fig. 3). With $n = 3$ in equation (5.33), we have

$$\left(\frac{\partial v}{\partial z}\right)_0 \frac{\Delta t}{2} = \left(-v_3 + S_3 \frac{\Delta t}{2}\right) \Big/ A_{z0,3} . \tag{6.45}$$

Thus, from equations (6.11), (6.41), (6.42), (6.44), and (6.45), B_{z0}, p_0, and ρ_0 are solved for by numerical iteration.

For corner point (III), the bicharacteristics number 3 and 4 are missing (see Fig. 3). Now $(u/r)_0 = 0$. With $n = 2$ in equation (5.28), we have

$$\left(\frac{\partial u}{\partial r}\right)_0 \frac{\Delta t}{2} = \left(-u_2 + Z_2 \frac{\Delta t}{2}\right) \Big/ A_{r0,2} . \tag{6.46}$$

Equation (5.26) reduces to

$$p_0 = T_5^f \Big/ \left\{1 + \gamma\left[\left(\frac{\partial u}{\partial r}\right)_0 + \left(\frac{\partial u}{\partial z}\right)_0\right]\frac{\Delta t}{2}\right\} . \tag{6.47}$$

Thus from equations (6.13), (6.41), (6.43), (6.46), and (6.47), B_{z0}, p_0, and ρ_0 are solved for by numerical iteration.

Similarly, for corner point (IV), the bicharacteristics number 1 and 4 are missing (see Fig. 3). Thus from equations (6.13), (6.41), and (6.45)–(6.47), B_{z0}, p_0, and ρ_0 are solved for by numerical iteration.

The accuracy of the results at the axis and boundary are compatible with that at the interior points.

VII. TEST CALCULATIONS AND NONLINEAR SIMULATIONS

The aim of our MHD code is to solve, for given initial data and boundary conditions, nonlinear two-dimensional wave propagation problems numerically. However, to test the validity of the code, we must compare the results of numerical calculations with those of known analytic solutions. Here we consider (*a*) linearized standing MHD wave motions in a magnetized cylindrical plasma; (*b*) nonlinear, self-similar expansion of a magnetized plasma ball; and (*c*) nonlinear evolution of large-amplitude standing MHD wave solutions.

a) *Linearized, Standing MHD Wave Motions in a Magnetized Cylindrical Plasma*

Consider a cylinder containing a magnetized plasma in a cylindrical coordinate system, with the z-axis the axis of the cylinder. In equilibrium, the constant background magnetic field $\boldsymbol{B}_0$ is parallel to the axis of the cylinder. Small perturbations with $b_\phi = 0$ and $v_\phi = 0$ are superposed on the back-

ground equilibrium. The boundary conditions are the following:

i) The normal perturbing velocities on the top, at the bottom, and on the side wall of the cylinder vanish;

ii) The normal perturbing magnetic fields on the side wall vanish;

iii) The tangential perturbing magnetic fields on the top and at the bottom of the cylinder vanish.

We have adopted condition (iii) because the corresponding eigenfunctions are of relatively simple form.

From the linearized MHD equations, with appropriate combinations (Lighthill 1960), it is straightforward to obtain the following propagating wave solutions for the axisymmetric case:

$$v_r = -A\frac{(c^2+a^2)(\omega^2-c_T^2k^2)}{\omega^2(\omega^2-a^2k^2)}mJ_0'(mr)e^{i\omega t+ikz}, \quad (7.1)$$

$$v_z = -iAk\frac{c^2}{\omega^2}J_0(mr)e^{i\omega t+ikz}, \quad (7.2)$$

$$p = Ai\frac{c^2}{\omega}\rho_0 J_0(mr)e^{i\omega t+ikz}, \quad (7.3)$$

$$\rho = A\frac{i\rho_0}{\omega}J_0(mr)e^{i\omega t+ikz}, \quad (7.4)$$

$$b_r = -\frac{A}{\omega}B_0 km\frac{(c^2+a^2)(\omega^2-c_T^2k^2)}{\omega^2(\omega^2-a^2k^2)}J_0'(mr)e^{i\omega t+ikz}, \quad (7.5)$$

$$b_z = iA\frac{B_0}{\omega}\left(1-\frac{c^2k^2}{\omega^2}\right)J_0(mr)e^{i\omega t+ikz}, \quad (7.6)$$

with the dispersion relation

$$\omega^4-(a^2+c^2)(m^2+k^2)\omega^2+a^2c^2k^2(m^2+k^2)=0 \quad (7.7)$$

(Roberts and Webb 1978; Wilson 1979), where

$$c^2=\frac{\gamma p_0}{\rho_0}, \quad (7.8)$$

$$a^2=\frac{B_0^2}{4\pi\rho_0}, \quad (7.9)$$

$$c_T^2=\frac{c^2a^2}{(c^2+a^2)} \quad (7.10)$$

(note the different notation used here for the sound speed and the Alfvén speed), $J_0(mr)$ is the zeroth-order Bessel function of the first kind, $J_0'(r)\equiv dJ_0(r)/dr$, A is a constant specifying the amplitude of the wave, and γ is the ratio of specific heats. The quantities with subscript zero are those of equilibrium; quantities without subscript zero are those related to the perturbations. An important property of dispersion relation (7.7) is that there always exist two positive roots for ω^2.

We consider standing wave solutions in a cylinder of height L and radius r_0 satisfying the boundary conditions (i), (ii), and (iii). In mathematical form, the boundary conditions (i), (ii), and (iii) are expressed as follows:

i) $v_z=0$ when $z=0$ and $z=L$; $v_r=0$ when $r=r_0$.

ii) $b_r=0$ when $r=r_0$;

iii) $b_r=0$ when $z=0$ and $z=L$.

A standing wave solution satisfying the boundary conditions (i), (ii), and (iii) is thus given by

$$v_r=\frac{M(\omega^2-c^2k^2)}{cmk}J_1(mr)\sin(\omega t)\cos(kz), \quad (7.11)$$

$$v_z=McJ_0(mr)\sin(\omega t)\sin(kz), \quad (7.12)$$

$$p=\frac{M\rho_0 c\omega}{k}J_0(mr)\cos(\omega t)\cos(kz), \quad (7.13)$$

$$\rho=\frac{M\rho_0\omega}{ck}J_0(mr)\cos(\omega t)\cos(kz), \quad (7.14)$$

$$b_r=\frac{MB_0J_1(mr)(\omega^2-c^2k^2)}{mc\omega}\cos(\omega t)\sin(kz), \quad (7.15)$$

$$b_z=\frac{MB_0J_0(mr)(\omega^2-c^2k^2)}{ck\omega}\cos(\omega t)\cos(kz), \quad (7.16)$$

where $J_1(r)$ is the Bessel functions of first order. In equations (7.11)–(7.16), $k=l\pi/L$ and $m=\beta_n/r_0$, where l is an integer and β_n $(n=1,2,\ldots)$ are zeros of $J_1(r)$.

To illustrate the results of the test calculation for standing wave solutions of equations (7.11)–(7.16), we choose parameters as follows: $r_0=10^7$ cm, $L=10^7$ cm, $l=1$, $\beta_1=3.8317059702$, $p_0=10^4$ dyne cm^{-2}, $B_0=10^3$ gauss, $\rho_0=10^{-7}$ g cm^{-3}, $M=10^{-6}$, and $\gamma=5/3$. For this set of parameters, dispersion relation (7.7) gives two characteristic periods of wave motions; the longer period is 52.2 s, and the shorter period is 13.3 s, corresponding to the slow and fast mode, respectively. Since the physical system is axisymmetric, the calculation is carried out over a spatial region $0<r<r_0$, $0<z<L$, where the 20 × 20 grid points are equally spaced in each dimension. The Courant time step $\sim$0.5 s. The calculation for the wave motion of shorter period (fast mode) is carried out for three periods, with the computational time step $\Delta t\approx 0.155\times 0.5$ s $=0.077$ s. Similarly, the calculation for the wave motion of longer period (slow mode) is carried out for four periods, with the computational time step $\Delta t\approx 0.082$ s. In addition, the code has been run for two other cases:

i) Mixing the fundamental modes of long and short periods;

ii) Mixing modes of short period with different wavelengths along z: $k_0=\pi/L$ and $k_1=2\pi/L$.

The computational time step for these latter two calculations is also $\Delta t\approx 0.077$ s, with a vertical Mach number $M=10^{-6}$. The background physical variables are the same as before.

Some examples of comparing simulation results with analytic results are shown in Figures 4, 5 and 6. The principal conclusions are the following:

1. The time step necessary for convergent results is approximately one-sixth that of the Courant time step for the present parameter regime.

2. In all cases, once a sufficiently small time step to achieve convergence is chosen, we find agreement between the simulation and the analytic results to at least two significant digits in all physical variables.

b) The Nonlinear Self-Similar Expansion of a Magnetized Ball

The general nonlinear self-similar solution of the ideal MHD equations with axisymmetry for $\gamma=4/3$ has been obtained by Low (1982). Although the treatment of Low (1982) includes gravitational stratification due to a point mass, the basic tech-

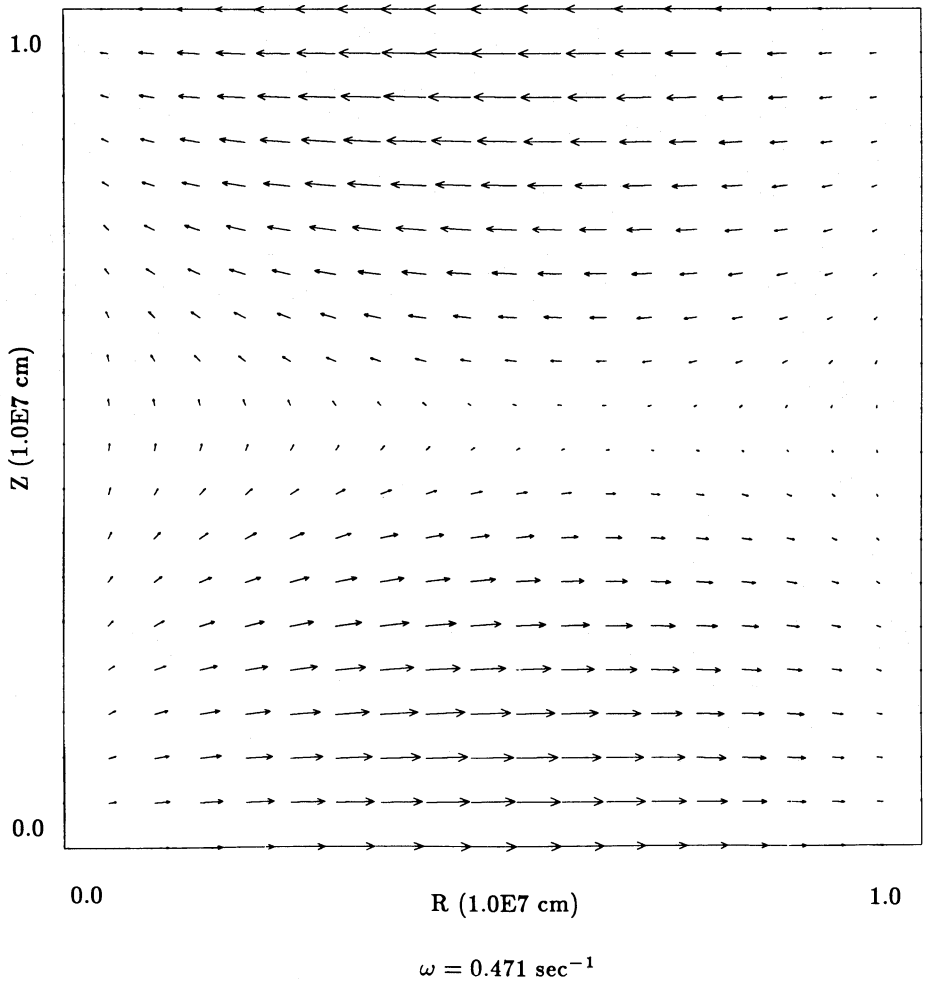

FIG. 4.—Typical two-dimensional flow pattern for a fast standing mode with a period of ~13.3 s at a fixed time. Arrows indicate the local direction of the velocity, and the length of the arrow is proportional to the magnitude of the local velocity. The maximum speed is ~2.43 cm s^{-1}, and all other speeds are normalized to this maximum. Parameters (defined in the text) used for this calculation are as follows: $r_0 = 10^7$ cm, $L = 10^7$ cm, $l = 1$, $\beta_1 = 3.8317059702$, $p_0 = 10^4$ dyne cm^{-2}, $B_0 = 10^3$ gauss, $\rho_0 = 10^{-7}$ g cm^{-3}, $M = 10^{-6}$, and $\gamma = 5/3$.

nique to obtain self-similar solutions applies in the absence of gravity. We are interested in the expansion of a magnetized plasma ball whose toroidal magnetic field and gravity vanish. The relevant MHD equations are given by equations (2.1)–(2.5).

In a spherical coordinate system (r, θ, ϕ), we define a self-similar radial variable

$$\zeta = r/\Phi\,, \tag{7.17}$$

where Φ is a function of time t. It is assumed that the flows occurs only in the radial direction; i.e.,

$$\boldsymbol{v} = v_r(r, \theta, t)\hat{\boldsymbol{r}}\,. \tag{7.18}$$

Using the same reduction as in Low (1982), we obtain the equation for $\Phi(t)$,

$$\left(\frac{d\Phi}{dt}\right)^2 = \frac{\eta\Phi - 2\alpha}{\Phi}\,, \tag{7.19}$$

where η and α are two constants of integration. The radial velocity, the gas pressure, the density, and the magnetic field are given by

$$v_r = \frac{r}{\Phi}\frac{d\Phi}{dt}\,, \tag{7.20}$$

$$p = \Phi^{-4}P(\zeta, A)\,, \tag{7.21}$$

$$\rho = \Phi^{-3}D(\zeta, A)\,, \tag{7.22}$$

$$\boldsymbol{B} = \frac{1}{r\sin\theta}\left(\frac{1}{r}\frac{\partial A}{\partial\theta}\hat{\boldsymbol{r}} - \frac{\partial A}{\partial r}\hat{\boldsymbol{\theta}}\right), \tag{7.23}$$

where the functions P and D are quite arbitrary and the scalar A is assumed to have the form

$$A = A(\zeta, \theta)\,. \tag{7.24}$$

The θ-component of the momentum equation gives

$$\frac{\partial^2 A}{\partial\zeta^2} + \frac{\sin\theta}{\zeta^2}\frac{\partial}{\partial\theta}\left(\frac{1}{\sin\theta}\frac{\partial A}{\partial\theta}\right) + 4\pi\zeta^2\sin^2\theta\frac{\partial P(\zeta, A)}{\partial A} = 0\,. \tag{7.25}$$

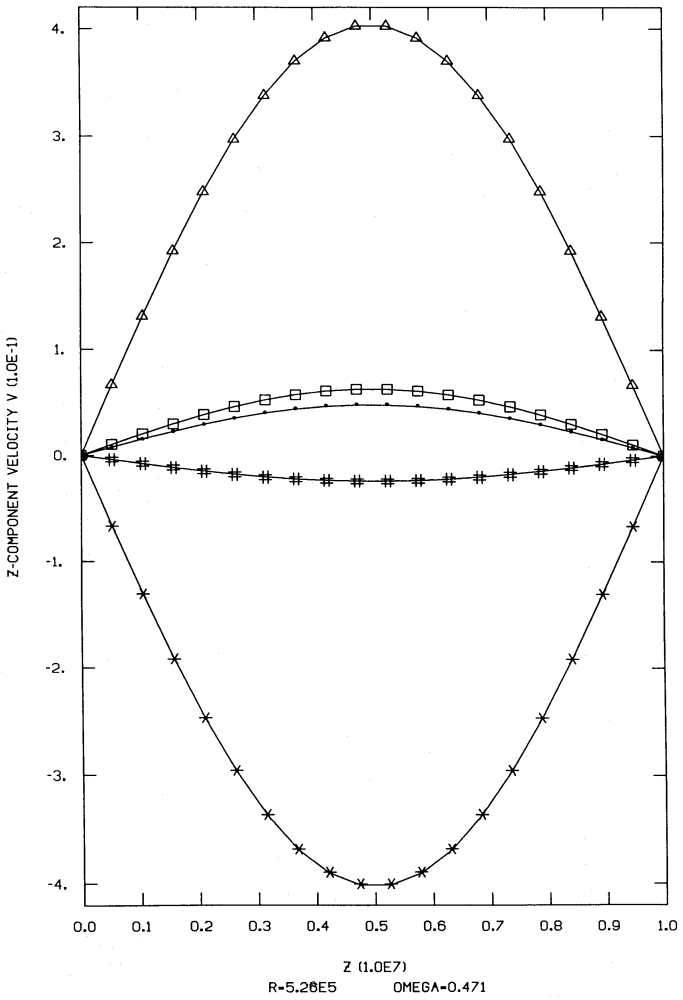

FIG. 5

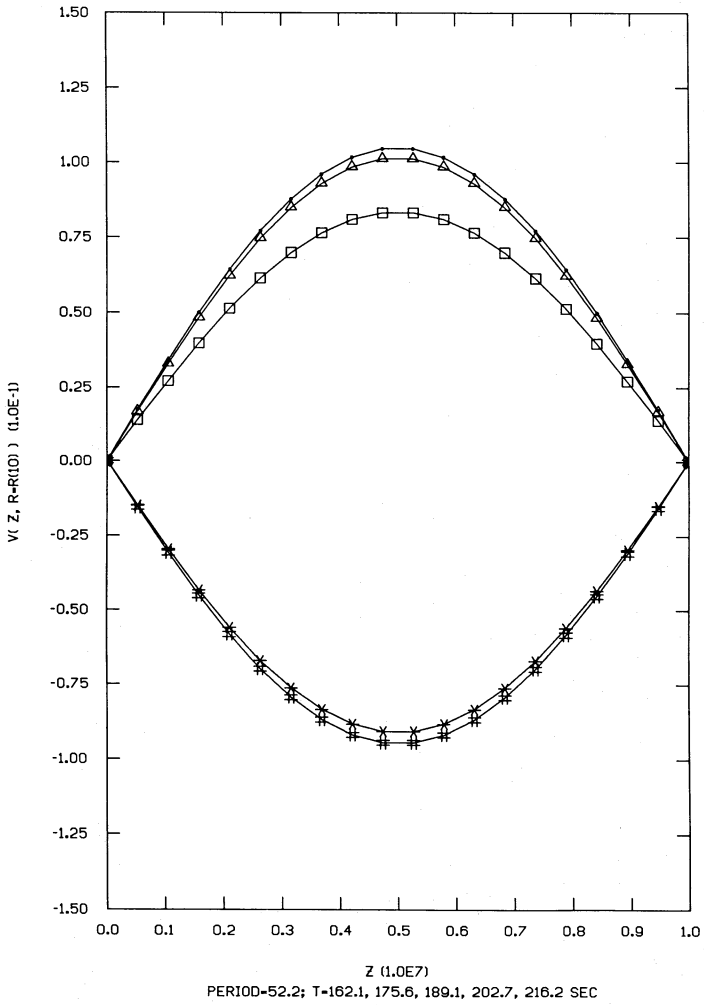

FIG. 6

FIG. 5.—Comparison of z-component velocity for the analytic solution and the results from the numerical code for a small-amplitude fast standing mode. Solid line represents the analytic results, and symbols represent the results from the code at various times: square, triangle, number symbol (#), asterisk, and dot are at times $t = 0.3315$, 3.3984, 6.7987, 10.1951, and 13.5935 s, respectively. The variation along the z-coordinate of the z-component velocity is shown for fixed $r = 5.26 \times 10^5$ cm. All parameter values are as in Fig. 4.

FIG. 6.—Linear asymmetric initial perturbation. Comparison of the analytic solution (*solid line*) and the results from the code (*symbols*) for the z-component velocity along the z-coordinate for a standing slow mode (with period 52.2 s) at a fixed radial location, $r = R(10) = 4.73 \times 10^6$ cm. Square, triangle, number symbol (#), asterisk, and dot are at times $t = 162.127$, 175.638, 189.148, 202. 659, and 216.169 s, respectively. All parameter values are as in Fig. 4.

The r-component of the momentum equation gives

$$\frac{\partial P(\zeta, A)}{\partial \zeta} + \alpha \zeta D(\zeta, A) = 0 . \quad (7.26)$$

To construct an exact self-similar solution for the given solution Φ of equation (7.19), we first prescribe the function $P(\zeta, A)$ and then solve equation (7.25) for $A(\zeta, \theta)$ subject to the appropriate boundary conditions. Thus the velocity, the gas pressure, the density, and the magnetic field are obtained by using equations (7.20)–(7.23), and (7.26).

One particular self-similar solution is constructed as follows. Assume $P(\zeta, A)$ is of the form:

$$P(\zeta, A) = f(\zeta)A + g(\zeta) . \quad (7.27)$$

For D to be positive, we require $g(\zeta)$ to be monotonically decreasing. It is also required that $dg(\zeta)/d\zeta = 0$ at $\zeta = 0$ so that the gradient (in the direction perpendicular to the axis) of the total pressure (gas plus magnetic) vanish on the axis of symmetry. Now equation (7.25) takes the form

$$\frac{\partial^2 A}{\partial \zeta^2} + \frac{\sin\theta}{\zeta^2}\frac{\partial}{\partial \theta}\left(\frac{1}{\sin\theta}\frac{\partial A}{\partial \theta}\right) + 4\pi\zeta^2 \sin^2\theta f(\zeta) = 0 . \quad (7.28)$$

Furthermore, we assume $A(\zeta, \theta)$ is of the separable form

$$A(\zeta, \theta) = F(\zeta) \sin^2\theta . \quad (7.29)$$

Equation (7.28) then reduces to an ordinary differential equation for $F(\zeta)$:

$$\frac{d^2F}{d\zeta^2} - \frac{2F}{\zeta^2} + 4\pi\zeta^2 f(\zeta) = 0 . \quad (7.30)$$

From equations (7.23) and (7.29), we must require

$$F(\zeta_0) = \left.\frac{dF}{d\zeta}\right|_{\zeta=\zeta_0} = 0 \quad (7.31)$$

for $\boldsymbol{B} = 0$ at $\zeta = \zeta_0$. On the other hand, geometric consideration requires B_r to be finite at $r = 0$, so that

$$F(0) = 0 . \quad (7.32)$$

Now we have freedom to choose $F(\zeta)$ (satisfying conditions [7.31] and [7.32]) and $g(\zeta)$ so that the pressure and the density are positive quantities.

For our test calculations, we choose

$$F(\zeta) = F_0 \zeta^2(\zeta^2 - a^2)^2 , \quad (7.33)$$

$$g(\zeta) = \frac{F_0^2}{\pi} a^6(a^2 - \zeta^2) , \quad (7.34)$$

where F_0 and a are positive constants. Thus for $\zeta \le a$, from equations (7.26), (7.27) and (7.29)–(7.32), we obtain

$$v_r = \frac{r}{\Phi}\frac{d\Phi}{dt} , \quad (7.35)$$

$$p = \Phi^{-4}\frac{F_0^2}{\pi}[(5a^2 - 7\zeta^2)(\zeta^2 - a^2)^2\zeta^2 \sin^2\theta + a^6(a^2 - \zeta^2)] , \quad (7.36)$$

$$\rho = \Phi^{-3}\frac{2F_0^2}{a\pi}[7\zeta^2(\zeta^2 - a^2)^2 \sin^2\theta + a^6] , \quad (7.37)$$

$$B_r = \Phi^{-2}2F_0 \cos\theta(\zeta^2 - a^2)^2 , \quad (7.38)$$

$$B_\theta = -\Phi^{-2}2F_0 \sin\theta(\zeta^2 - a^2)(3\zeta^2 - a^2) . \quad (7.39)$$

In a cylindrical coordinate system (r, ϕ, z), the equivalent form of solutions (7.35)–(7.39) is

$$v_r = \Phi^{-1}\left[\frac{\eta\Phi - 2\alpha}{\Phi}\right]^{1/2} r , \quad (7.40)$$

$$v_z = \Phi^{-1}\left[\frac{\eta\Phi - 2\alpha}{\Phi}\right]^{1/2} z , \quad (7.41)$$

$$p = \Phi^{-4}\frac{F_0^2}{\pi}\left\{\left[5a^2 - 7\frac{(z^2 + r^2)}{\Phi^2}\right]\left[\frac{(z^2 + r^2)}{\Phi^2} - a^2\right]^2 \times \frac{r^2}{\Phi^2} + a^6\left[a^2 - \frac{(z^2 + r^2)}{\Phi^2}\right]\right\} , \quad (7.42)$$

$$\rho = \Phi^{-3}\frac{2F_0^2}{\alpha\pi}\left\{7\frac{r^2}{\Phi^2}\left[\frac{(z^2 + r^2)}{\Phi^2} - a^2\right]^2 + a^6\right\} , \quad (7.43)$$

$$B_r = \frac{4F_0}{\Phi^4}\left[a^2 - \frac{(z^2 + r^2)}{\Phi^2}\right]rz , \quad (7.44)$$

$$B_z = \frac{2F_0}{\Phi^2}\left[\frac{(z^2 + r^2)}{\Phi^2} - a^2\right]\left[\frac{(z^2 + 3r^2)}{\Phi^2} - a^2\right] . \quad (7.45)$$

By solving equation (7.19) for $\alpha > 0$ and $\eta > 0$, we have

$$t - t_0 = \frac{1}{\eta}\sqrt{\Phi(\eta\Phi - 2\alpha)} + \frac{2\alpha}{\eta\sqrt{\eta}}\log(\sqrt{\eta\Phi} + \sqrt{\eta\Phi - 2\alpha}) , \quad (7.46)$$

where t_0 is the constant of integration (Low 1982). We require that when $t = 0$, then $\Phi = 2\alpha/\eta$; hence, the constant of integration t_0 is

$$t_0 = -\frac{\alpha}{\eta\sqrt{\eta}}\log(2\alpha) . \quad (7.47)$$

Equation (7.46) can be used to express Φ as a function of t numerically. The self-similar evolution of the magnetized plasma ball is therefore determined by equations (7.40)–(7.46) for given parameters α, η, F_0, and α.

For the test calculation, we choose the parameters: $\alpha = 2 \times 10^{-7}$ s^2, $\eta = 4 \times 10^{-7}$ s^2, $F_0 = 3 \times 10^{-18}$ gauss cm^{-4}, and $a = 5 \times 10^4$ cm. The spatial domain of the calculation is 100×100 cm^2. For the given set of parameters, the variable Φ is of order 1; from equations (7.39)–(7.46), we estimate that the flow velocity $v \approx 30$ cm s^{-1}, the gas pressure $p \sim 100$ dyne cm^{-2}, the density $\rho \approx 0.1$ g cm^{-3}, and the magnetic field $B \approx 30$ gauss. We start the calculation at $t = 2000$ s. The actual time step is $\Delta t = 0.05$ s, and the number of time steps is 50. The actual expansion is quite slow: the analytic solution shows that the values of the physical variables differ between adjacent time steps only for digits after the first five to six significant digits. This calculation is therefore an exacting test of numerical stability for our code.

The results of the calculation at each time step have 10–11 digit agreement with the analytic solution. We have explored the different parts of the spatial domain of the physical system by moving the computing domain: the accuracy of the calculation in different parts of the physical system is always comparable.

In this test example, we do not have physical boundary conditions (because we consider a similarity solution). The physical variables at each time step on the computational boundary are therefore calculated by using the analytic solu-

tion. The purpose of this test calculation is thus only to show that the numerical procedure using the method of characteristics yields highly accurate and stable results for the interior points of the computing domain.

c) Nonlinear Evolution of Large-Amplitude Standing MHD Waves

In text example *a*, we have tested the linear behavior of the code for both fast and slow modes; in test example *b*, we have tested the nonlinear behavior of the code for very short periods of time with high spatial resolution. To further test the quality of our code, we have simulated the evolution of standing MHD waves (see test example *a*), but with large initial amplitudes. It is natural to expect that the numerical results will deviate from the scaled linearized standing MHD wave solutions (which are plotted in the Figs. 7, 8, 9 as reference) as time goes on because nonlinear effects will make their presence felt.

We have run the nonlinear simulations for several cases with the same background physical parameters as provided in test example *a*. In all the following cases, the periods refer to those for the linearized standing wave solutions.

1. Slow mode calculation for four periods, with $M = 10^{-1}$

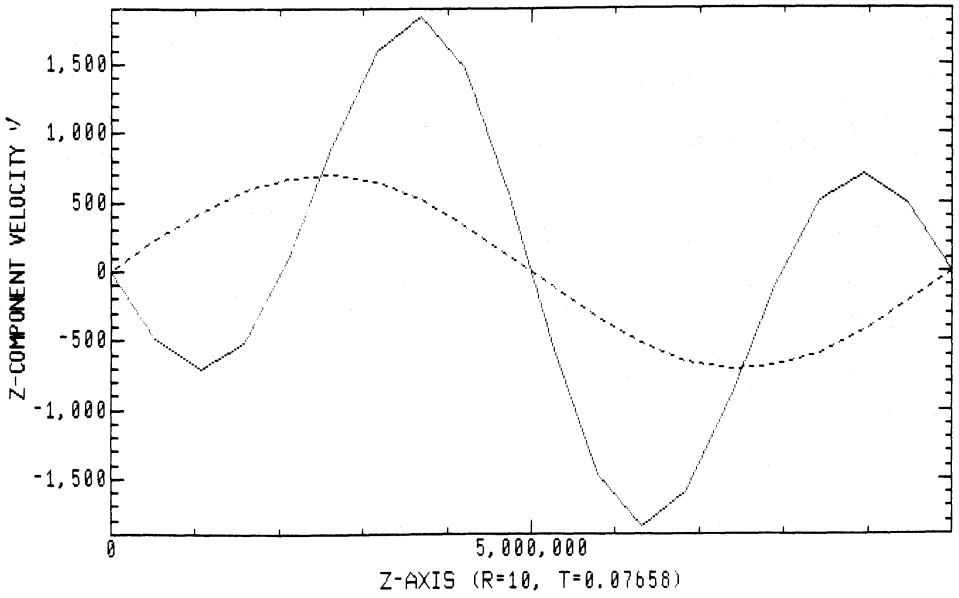

FIG. 7*a*

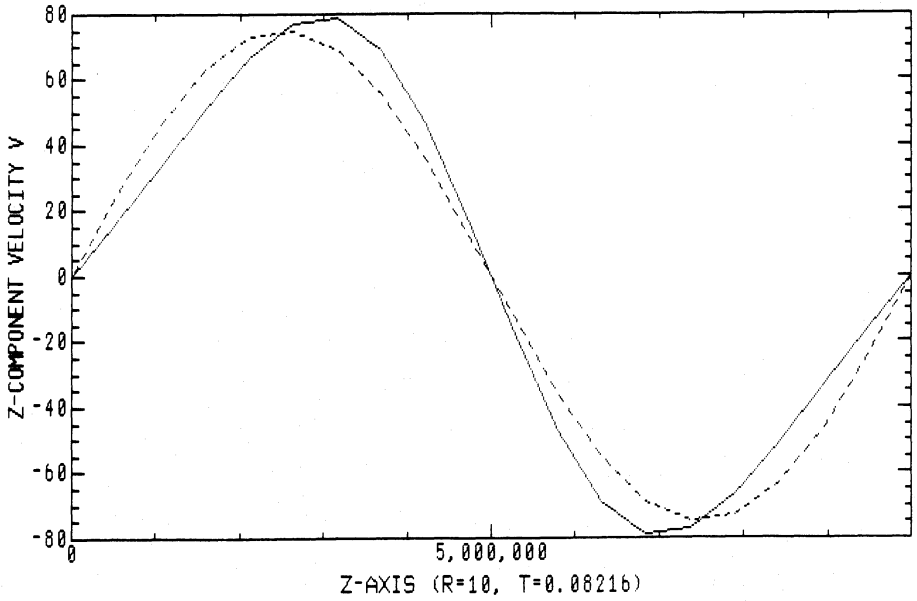

FIG. 7*b*

FIG. 7.—Comparison between the computational results (*solid line*), using a large-amplitude fast mode as the initial perturbation, and the corresponding linearized standing MHD fast mode solution (of period 9.3 s) whose amplitude is scaled appropriately for comparison (*dashed line*). We show the variations of the z-component velocity along z-coordinate at radial location $r = 4.73 \times 10^6$ cm (which corresponds to $R = 10$ in the figures). Here $l = 2$ (symmetric perturbation about the center of the cylinder) and $M = 10^{-1}, 10^{-2}$ for (*a*) and (*b*), respectively. All other parameter values are as in Fig. 4.

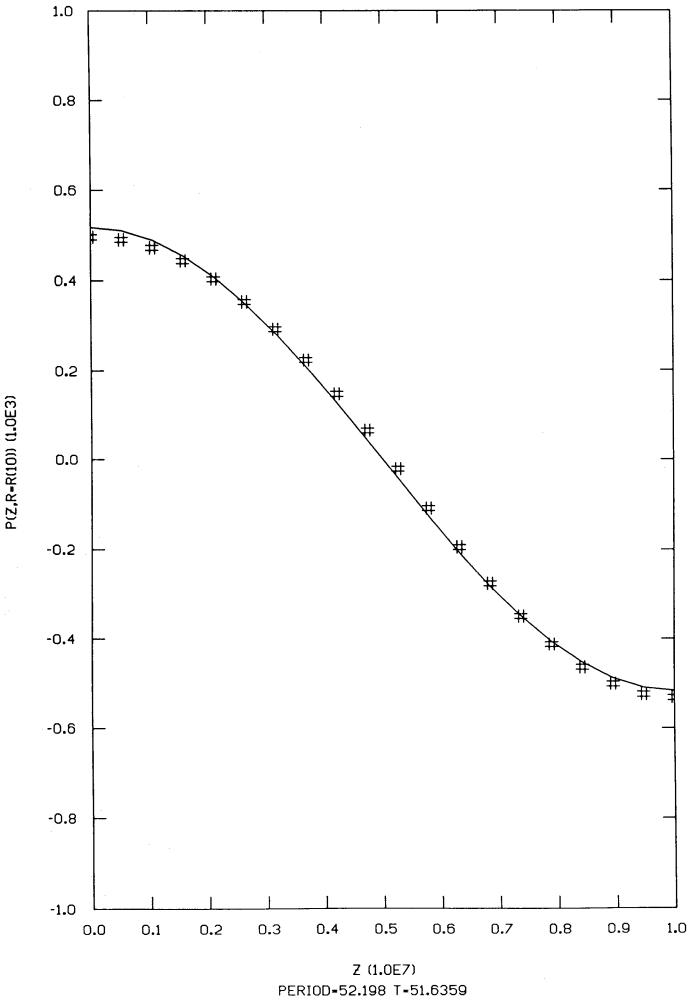

FIG. 8*a*

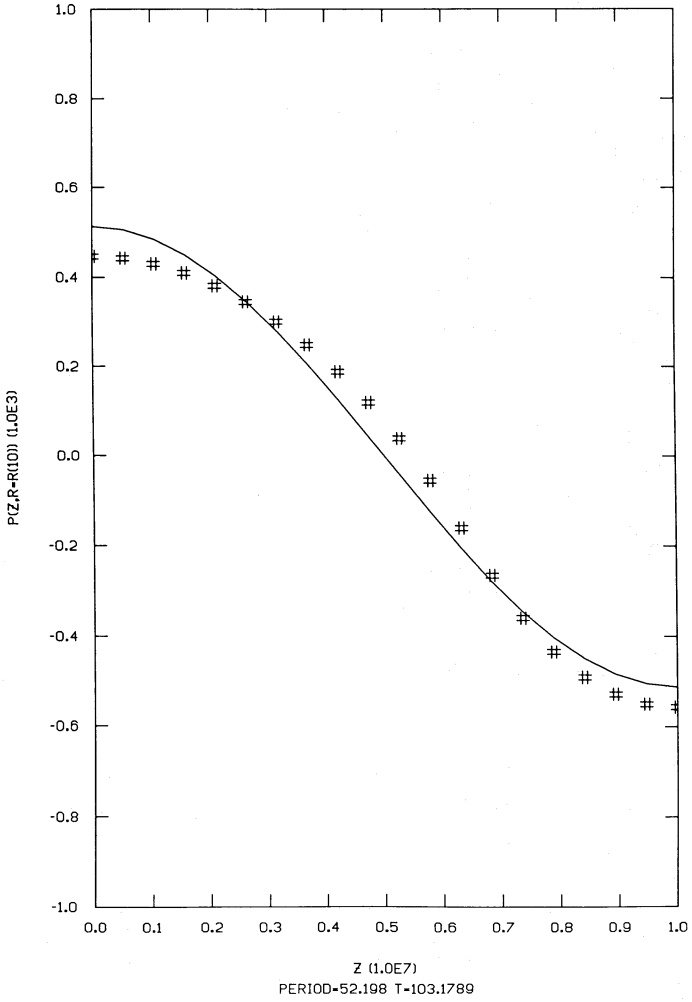

FIG. 8*b*

FIG. 8.—Nonlinear asymmetric initial perturbation. Comparison between the computational result for the gas pressure perturbation along the z-coordinate at a radial location of $r = 4.73 \times 10^6$ cm, using a large-amplitude slow mode as the initial perturbation (#), and the corresponding linearized standing MHD slow mode solution (of period 52.2 s) whose amplitude is again scaled appropriately for comparison (*solid curve*). Here $l = 1$ (asymmetric perturbation about the center of the cylinder), $M = 10^{-1}$, and the times displayed are at times $t = 51.63, 103.18, 154.50, 205.62$ s. All other parameter values are as in Fig. 4.

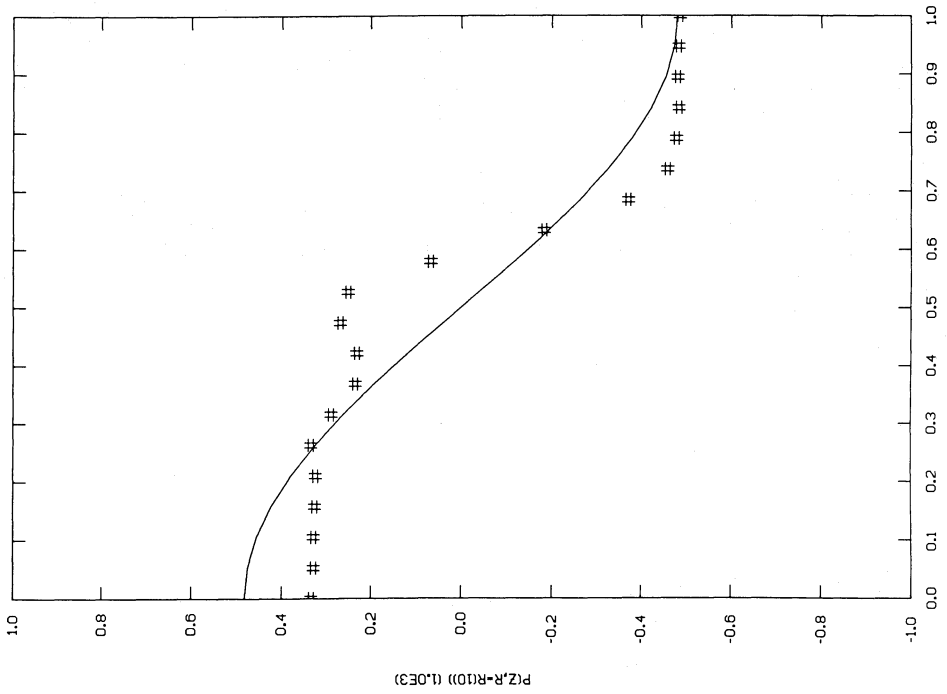

FIG. 8*d*

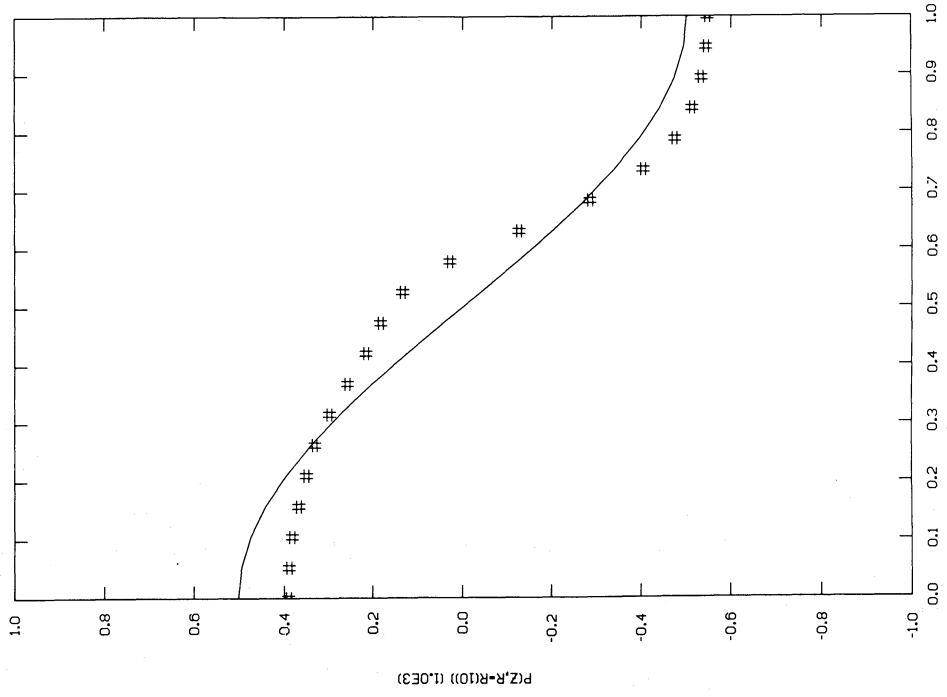

FIG. 8*c*

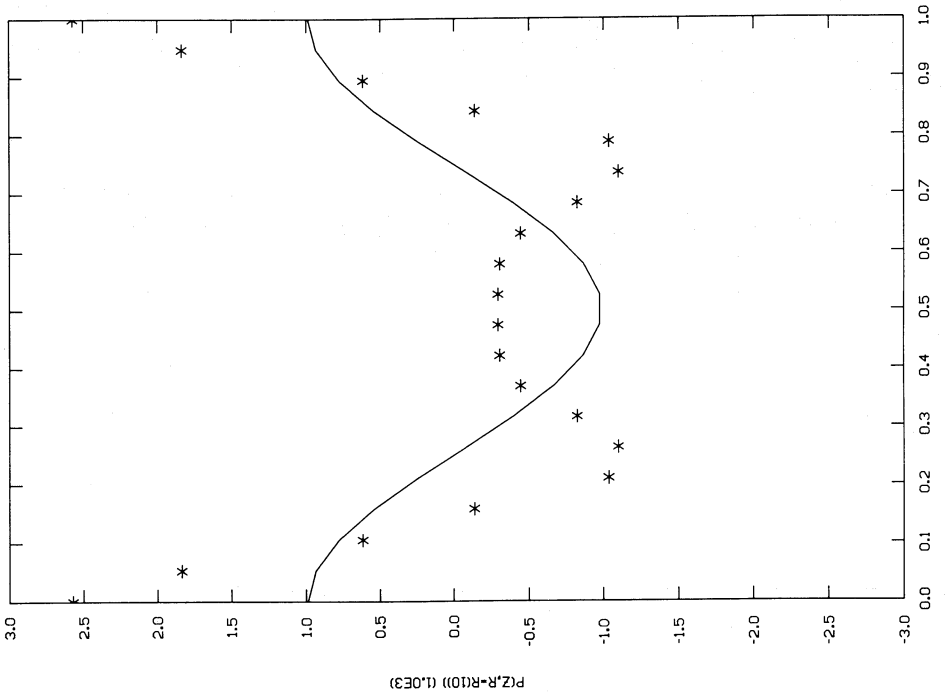

FIG. 9b

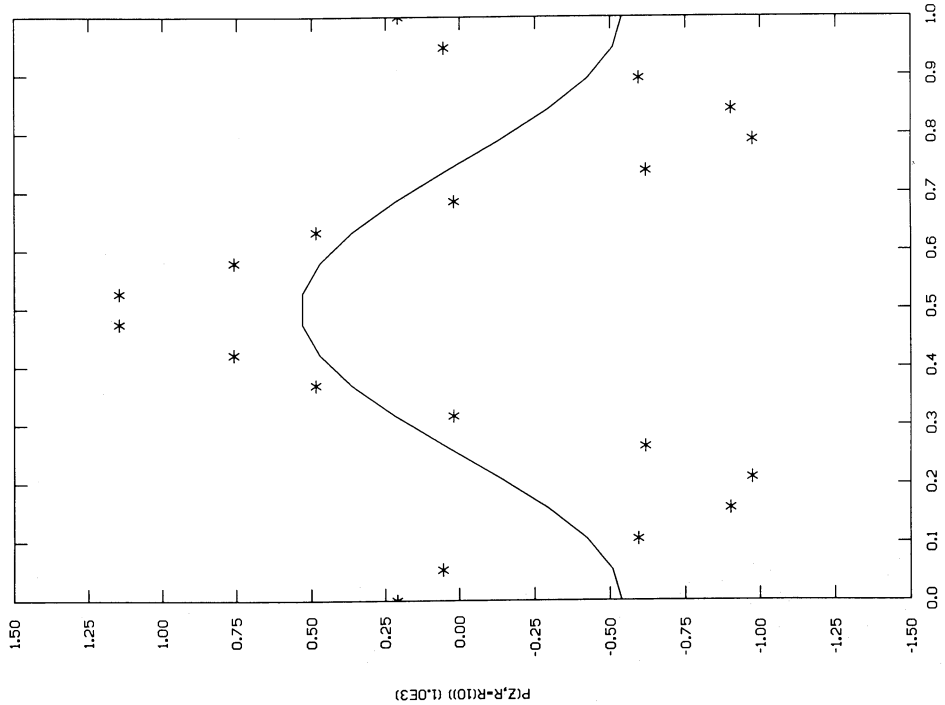

FIG. 9a

FIG. 9.—Nonlinear symmetric initial perturbation. Comparison between the computational result for the gas pressure perturbation along the z-coordinate at a radial location of $r = 4.73 \times 10^6$ cm (*asterisk*), using a large-amplitude fast mode as the initial perturbation, and the corresponding linearized standing MHD fast mode solution (of period 9.27 s) whose amplitude is scaled appropriately for comparison (*solid line*). Here $l = 2$ (symmetric perturbation about the center of the cylinder), $M = 10^{-1}$, and the times displayed are at $t = 24.93$, 29.03, 35.06, 39.16 s. All other parameter values are as in Fig. 4.

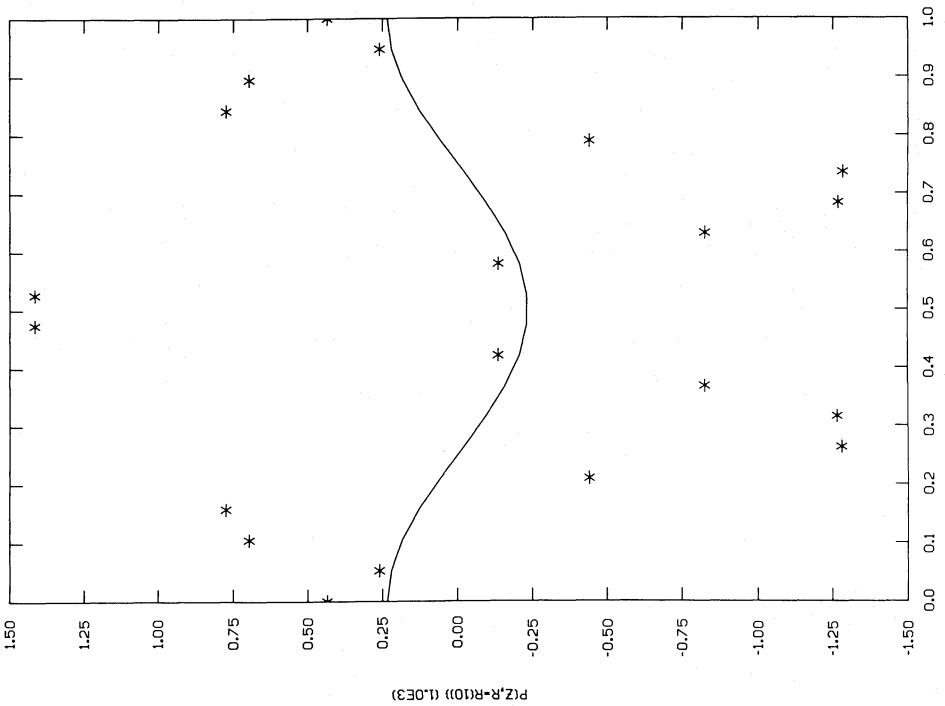

FIG. 9*d*

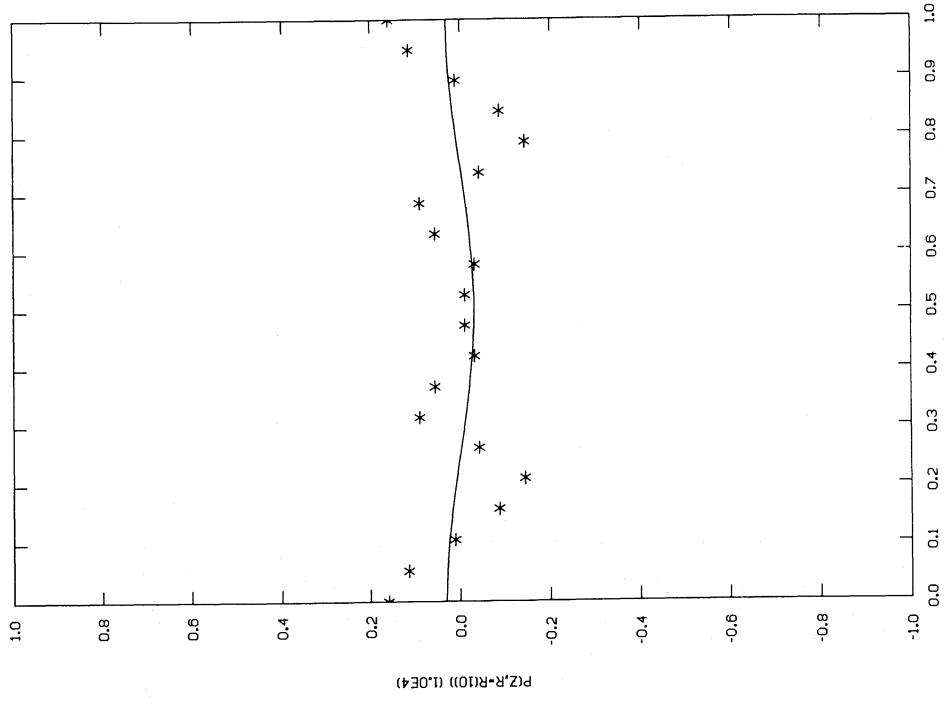

FIG. 9*c*

and $k = \pi/L$; i.e., the initial perturbation is physically asymmetric about the center of the cylinder in the longitudinal sense; the computational time step is $\Delta t \approx 0.079$ s.

2. Fast mode calculation for four periods, with $M = 10^{-1}$ and $k = \pi/L$; the computational time step is $\Delta t \approx 0.067$ s.

3. Fast mode calculation for four periods, with $M = 10^{-1}$ and $k = 2\pi/L$; i.e., the initial perturbation is physically symmetric about the center of the cylinder in the longitudinal sense; the computational time step is $\Delta t \approx 0.067$ s.

For all calculations, stably convergent results are obtained. It is shown by the nonlinear simulations that initially symmetric perturbations retain their symmetry in time. By gradually changing the initial amplitudes, we have traced out the form of the deviations from linear behavior as nonlinear effects come into play; as we will show below, our results agree with order-of-magnitude estimates of the nonlinear effects and indicate correct qualitative behavior. In addition, we have carefully examined the conservation of energy, mass, and magnetic flux, and find that the conservation laws are satisfied to the accuracy of the numerical differencing scheme.

In order to set the stage for analysis of the nonlinear calculation, we first focus on the linear results. In Fig. 4, we show a two-dimensional standing flow pattern for a fast mode in the linearized regime at a fixed time. For this specific example, the flow pattern oscillates at period 13.3 s; when the flow speed diminishes, the associated kinetic energy is transformed into compressional and magnetic energies, and vice versa. It is worth noting that for the fast mode, the gradients of gas pressure and of magnetic pressure are roughly in the same direction, whereas for the slow mode, the two gradients point in the approximately opposite direction. The general small-amplitude flow pattern is, of course, a superposition of all possible (linear) eigenmodes.

In Figure 5, we illustrate the extent of agreement between the computational results and the analytical solution for a fast mode in the linear regime near the symmetry axis. It is evident that the code behaves very well in the linear domain for the fast mode—which is a minimal necessary condition for a good code.

In Figure 6, we similarly compare the computational results and the analytical solution for a slow mode in the linear regime, at a location roughly halfway between the symmetry axis and the wall. The excellent linear behavior of the nonlinear code for the slow mode should not be surprising—we have already explained the reason for using the fast cone alone in detail in § II; these numerical results substantiate this theoretical argument.

In Figure 7, we compare the computational results and the analytical solution for the fast mode at a radius roughly halfway between the symmetry axis and the wall for various values of the initial perturbation amplitude. The perturbation in this case is reflectionally symmetric (in z) about the center of the cylinder. We only plot the z-component velocity for comparison; all other physical variables do not sensibly deviate from the analytic solution after the first integration time step.

The first point to note is that there is significant disagreement between the analytic and computational results for large initial perturbation amplitudes (Fig. 7*a*), but that as the initial amplitude is reduced (Figs. 7*a*, 7*b*), the disagreement gradually disappears. Since the computational results are smooth and show the proper symmetry, we may fairly ask whether the discrepancies of large initial amplitudes are physically correct and reflect the action of nonlinearities. Let us then consider the z-component momentum equation (2.7) term by term at the first computed time step for the case shown in Figure 7*a*. Since we start the initial perturbation with zero velocity, the second and the third terms in equation (2.7) are not important, the fourth linear term $(1/\rho)(\partial p/\partial z) \approx 9000$, the fifth nonlinear term $(B_r/4\pi\rho)(\partial B_r/\partial z) \approx 20{,}000$, and the sixth nonlinear term $(B_r/4\pi\rho)(\partial B_z/\partial r) \approx 4000$. From these estimates, it is obvious that large nonlinear effects are to be expected. From equation (7.15) at small t, we see that the nonlinear term $(B_r/4\pi\rho)(\partial B_r/\partial z)$ should dominantly determine the functional form of v_z; indeed the computational result shown in Figure 7*a* indicates a nodal structure identical to this dominant driving term, as expected. Actually this very case shows how a nonlinear equation generates higher harmonics. The consistency of this description can be tested by reducing the initial amplitude by a factor of 10, as in Figure 7*b*; the single linear term in equation (2.7) is then reduced by the same factor, but all the nonlinear terms are reduced by a factor of 100. Thus, we see immediately that the linear term ought to dominate, and in fact the discrepancy between the linear analytic solution and the computed result is sharply reduced, an effect which becomes more pronounced as the initial amplitude is reduced yet further. Why do the other physical variables not show similar nonlinear effects after the first integration time step even when the initial amplitude is large? When one examines equations (2.6), (2.8), (2.10), (2.11), and (2.13) carefully, the answer is simply that in the evolution equations for all variables other than the z-component velocity, there always exist linear terms which dominate the nonlinear terms for the entire range of initial perturbation amplitudes shown in Figure 7.

In order to illustrate further the nonlinear evolution of these standing waves, we show the evolution for a MHD slow mode of the gas pressure perturbation in Figure 8. For reference, we also plot the corresponding analytic solution scaled to the appropriate (large) amplitude; keep in mind that this is done only to highlight the nature of the nonlinear wave evolution, and that the actual solution lies well in the nonlinear domain. We find that the nonlinear calculation is quite stable as we observe the gradual steepening of the perturbation as the system oscillates back and forth. The way of steepening is exactly as one would expect as the sound speed increases locally with increasing pressure. At times $t = 180.07$ s and $t = 205.62$ s, we see ripples which we believe are the result of back reflections due to the steepening. Since we have not implemented shock treatment in the present code, we stopped the calculation at the indicated time.

In Figure 9, we show the nonlinear evolution for a MHD fast mode of the gas pressure perturbation. Again, the nonlinear numerical calculation is stable. The results are physically symmetric about the center of the cylinder, consistent with the initial perturbations and the expected nonlinear evolution. We again see the clear effects of generation of higher harmonics and the resulting wave steepening. We have examined the conservation of energy, mass, and magnetic flux, and we find these conserved to three significant digit accuracy (consistent with expectations based on the accuracy of the differencing scheme and with our experience with the linear calculations).

VII. DISCUSSION AND SUMMARY

We have developed a two-dimensional MHD computational code using the method of characteristics and have shown that it is highly accurate and stable. Its present capabilities are demonstrated by solving two very different problems

for which analytical solutions exist, and by considering nonlinear simulations of large-amplitude standing MHD waves. Aside from coding complexity, the most difficult problem encountered is the numerical treatment of the boundary points for various physical boundary conditions; nevertheless, it is straightforward to carry out modifications of the treatment at the boundary, although, in general, the accuracy at the boundary is always slightly less than that for interior points. This is because the cubic spline interpolation scheme requires the normal derivatives of the physical variables at the boundary: for certain boundary conditions, the normal derivatives at the boundary are given, but for other boundary conditions, the normal derivatives at the boundary are not; in the latter case, we have to use the ratio of the finite differences to approximate the normal derivatives at the boundary. The error introduced by this procedure turns out to be relatively unimportant in the interior.

An important feature of the present scheme is that as long as the interpolation is given for all the grid points, the numerical iterations for solving for the physical variables at each grid point are entirely independent of each other. Thus, for supercomputers based on massively parallel architectures, the total computational time can be dramatically reduced.

We thank U. Bohn, B. C. Low, D. Mihalas, and D. Muchmore for their comments and suggestions during the course of this work, H. Spruit for several valuable suggestions on improving the paper, and the NCAR Consulting Service (Boulder, CO) and Mrs. Platte (Heidelberg) for assistance in computing access. This work was supported in part by the NASA Solar-Terrestrial Theory program at the Harvard-Smithsonian Center for Astrophysics, by National Science Foundation grant AST 85-06640 at Harvard University, and by the Deutsche Forschungsgemeinschaft (SFB 132). The computing was supported at NCAR by the NSF. Finally, we thank the High Altitude Observatory, and especially its director, R. MacQueen, for the hospitality afforded us during visits to NCAR.

REFERENCES

Courant, R., and Hilbert, D. 1962, *Methods of Mathematical Physics*, Vol. **2**, *Partial Differential Equations* (New York: Interscience).
Deinzer, W., Hensler, G., Schüssler, M., and Weisshaar, E. 1984, *Astr. Ap.*, **139**, 426.
Fletcher, C. A. J. 1984, *Computational Galerkin Methods* (New York: Springer).
Garabedian, P. R. 1964, *Partial Differential Equations* (New York: Wiley).
Gottlieb, D., and Orszag, S. A. 1977, *Numerical Analysis of Spectral Methods* (Philadelphia: SIAM).
Herbold, G., Ulmschneider, P., Spruit, H. C., and Rosner, R. 1985, *Astr. Ap.*, **145**, 157.
Jeffrey, T., and Taniuti, T. 1964, *Nonlinear Wave Propagation*, Vol. **9** (New York: Academic).
Lighthill, M. J. 1960, *Phil. Trans. Roy. Soc., London, A*, **252**, 397.
Low, B. C. 1982, *Ap. J.*, **254**, 796.
Mitchell, A. P. 1972, *J. Inst. Math. Appl.*, **9**, 378.
Richardson, D. J. 1964, *Meth. Comput. Phys.*, **3**, 295.
Richtmyer, R. D. 1957, *Difference Methods for Initial-Value Problems* (New York: Interscience).
Roache, P. J. 1976, *Computational Fluid Dynamics* (Albuquerque: Hermosa).
Roberts, B., and Webb, A. R. 1978, *Solar Phys.*, **56**, 5.
Shin, Y. W., and Kot, C. A. 1978, *J. Comput. Phys.*, **28**, 211.
Shin, Y. W., and Valentin, R. A. 1976, *J. Comput. Phys.*, **20**, 220.
Späth, H. 1973, *Spline-Algorithmen zur Konstruktion glatter Kurven und Flächen* (München: Oldenburg).
Spruit, H. C. 1981, in *The Sun as a Star*, ed. S. Jordan (NASA SP-450), p. 385.
Spruit, H. C., and Roberts, B. 1983, *Nature*, **304**, 401.
Stefanik, R. P., Ulmschneider, P., Hammer, R., and Durrant, C. J. 1984, *Astr. Ap.*, **134**, 77.
Stix, T. H. 1962, *The Theory of Plasma Waves* (New York: McGraw-Hill).
Von Neumann, J., and Richtmyer, R. D. 1950, *J. Appl. Phys.*, **21**, 232.
Wilson, P. R. 1979, *Astr. Ap.*, **71**, 9.

Y. Q. Lou: Physics Department, Harvard University, Cambridge, MA 02138

R. Rosner: Harvard-Smithsonian Center for Astrophysics, 60 Garden Street, Cambridge, MA 02138

P. Ulmschneider: Institut für Theoretische Astrophysik, Im Neuenheimer Feld 294, D-6900 Heildelberg, West Germany